Cell Reports

Article

Dose-dependent mitochondrial H_2O_2 signaling drives toxicity or stress adaptation and longevity in fission yeast

Graphical abstract

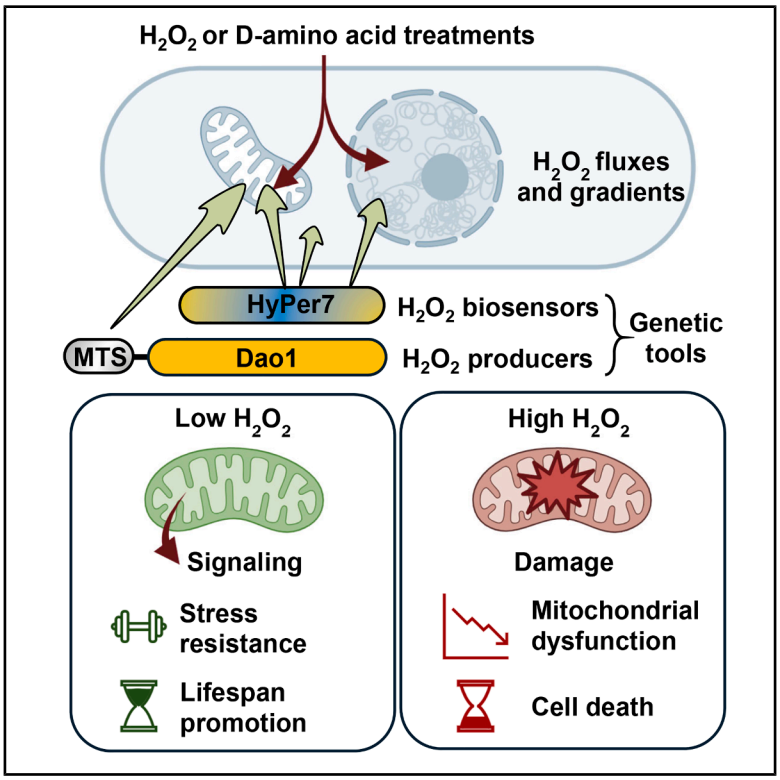

Highlights

- HyPer7 in different compartments revealed 2- to 5-fold H_2O_2 fluxes across membranes
- H_2O_2 produced by mitochondrial-targeted Dao1 can reach the nucleus
- High mitochondrial H_2O_2 levels disrupt mitochondrial morphology and respiration
- Low mitochondrial H_2O_2 levels boost stress resistance and extend lifespan

Authors

Laura de Cubas, María Florencia Crevatin, Montserrat Vega, Susanna Boronat, José Ayté, Elena Hidalgo

Correspondence

elena.hidalgo@upf.edu

In brief

Using fission yeast, we controlled and monitored intracellular H_2O_2 to study its spatiotemporal signaling. Localized mitochondrial H_2O_2 reached the nucleus and, depending on intensity, either enhanced stress resistance and longevity or impaired mitochondrial function. These findings define a quantitative framework for mitochondrial redox signaling and its impact on cellular fitness.

de Cubas et al., 2026, Cell Reports *45*, 117277
April 28, 2026
https://doi.org/10.1016/j.celrep.2026.117277

CellPress

Cell Reports

CellPress
OPEN ACCESS

Article

Dose-dependent mitochondrial H_2O_2 signaling drives toxicity or stress adaptation and longevity in fission yeast

Laura de Cubas,[1,2,3] María Florencia Crevatin,[1,3] Montserrat Vega,[1] Susanna Boronat,[1] José Ayté,[1] and Elena Hidalgo[1,4,*]
[1]Oxidative Stress and Cell Cycle Group, Universitat Pompeu Fabra, C/ Dr. Aiguader 88, 08003 Barcelona, Spain
[2]Present address: Division of Redox Regulation, German Cancer Research Center (DKFZ), DKFZ-ZMBH Alliance, 69120 Heidelberg, Germany
[3]These authors contributed equally
[4]Lead contact
*Correspondence: elena.hidalgo@upf.edu
https://doi.org/10.1016/j.celrep.2026.117277

SUMMARY

The spatiotemporal dynamics of hydrogen peroxide (H_2O_2) signaling and its effects on gene expression and cell fitness remain unclear. Using fission yeast, we applied genetic tools to control and monitor intracellular H_2O_2 levels. We expressed the H_2O_2 biosensor HyPer7 in four subcellular compartments, overexpressed D-amino acid oxidase (Dao1) in specific locations to induce localized H_2O_2 production, and modulated H_2O_2 detoxification or sensing. H_2O_2 concentrations showed 2- to 5-fold reductions across membranes, and D-amino acid treatments generated nanomolar H_2O_2 levels in Dao1-expressing cells. Mitochondrial-targeted Dao1 produced H_2O_2 fluxes capable of reaching the nucleus. While high mitochondrial H_2O_2 disrupted mitochondrial morphology and respiration, lower levels triggered antioxidant defenses, enhancing stress resistance and longevity. These findings establish a quantitative framework for mitochondrial H_2O_2 signaling and demonstrate that localized redox signals from mitochondria can either promote or impair cellular fitness depending on their intensity.

INTRODUCTION

High hydrogen peroxide (H_2O_2) levels can cause toxicity, whereas moderate increases can activate signaling pathways (reviews are available elsewhere[1–5]). The production and scavenging of H_2O_2 determine its steady-state levels and control peroxide fluxes between different cellular compartments.

Although the quantitative contribution of mitochondria to the final levels of H_2O_2 remains unknown, this organelle is recognized as a major source of reactive oxygen species (ROSs). Both electron transport chain (ETC) components and other mitochondrial enzymes contribute to H_2O_2 production (for a review, see Murphy[6]). When derived from the ETC, H_2O_2 is generated through the spontaneous or superoxide dismutase-catalyzed dismutation of superoxide. Other significant sources of H_2O_2 include NADPH oxidases, cytochrome P450 enzymes, and organelles such as the endoplasmic reticulum (for a review, see Holmström and Finkel[7]).

The molecular mechanisms that govern longevity, which often overlap with key hallmarks of health and cell fitness,[8,9] are highly conserved throughout evolution. Chronological lifespan (CLS), defined as the survival of non-proliferating cells, serves as an indicator of health and longevity in *Schizosaccharomyces pombe*. Calorie restriction enhances cell fitness and extends lifespan in most model organisms, making it one of the most widely recognized anti-aging interventions.[10] The effect of calorie restriction is most likely mediated by the inhibition of highly conserved nutrient-responsive kinases, target-of-rapamycin (TOR), and protein kinase A (PKA), alongside the activation of stress-regulated kinases such as Sty1 (for reviews, see Chen et al. and Dawes and Perrone[11,12]). Mitochondrial metabolism plays a crucial role in regulating CLS and is likely a downstream effector of caloric restriction. For several decades, the ETC has been regarded as the primary source of ROS,[13,14] and upregulation of mitochondrial respiration has been linked to the activation of stress responses and lifespan extension, likely mediated by physiological fluxes of H_2O_2 interacting with thiol switches in protein sensors.[15–18]

Both the synthesis and scavenging of H_2O_2 determine the steady-state levels of peroxides across space and time, regulating and limiting their inter-compartmental fluxes. There are two main families of H_2O_2 scavengers, classified by their reaction type: heme-based catalases and thiol-based peroxidases, which include glutathione peroxidases and thioredoxin peroxidases (peroxiredoxins).[19] The concentration, efficiency, and localization of these scavengers vary across different cell types. In fission yeast, the cytosolic and abundant peroxiredoxin Tpx1 serves as the primary H_2O_2 scavenger, exhibiting high sensitivity to peroxides under basal growth conditions. Cells lacking Tpx1 are unable to grow on solid plates under aerobic conditions[20]

due to an increase in cytosolic peroxide concentrations.[21,22] Catalase (Ctt1) is essential for survival in the presence of externally added peroxides, and its overexpression can fully or partially suppress the peroxide sensitivity of cells lacking components of antioxidant signaling cascades.[23]

Which is the contribution of H_2O_2 generation to the peroxide levels in compartments different from the main source? Cellular membranes have limited permeability to H_2O_2, and the concentration of peroxides at both sides of a given membrane will also depend on the compartment-specific scavenging activities, which further enhance the differences across the membrane. In the case of fission yeast, it has been experimentally demonstrated that the cytoplasmic membrane creates a permeability gradient of extracellular-to-intracellular peroxides of 40:1, and H_2O_2 scavenging by Tpx1 enhances the gradient up to 300:1.[22]

The transient nature of H_2O_2 and the constant generation and scavenging in different cellular locations do not facilitate the estimation of concentrations and gradients within the cell. In recent years, fluorescent protein-based reporters to measure intracellular H_2O_2 have been designed and optimized to demonstrate fluctuations of peroxides.[24,25] Two major families of genetically encoded redox reporters are commonly used: the reduction-oxidation-sensitive green fluorescent protein (roGFP)-based proteins fused to peroxiredoxins[21,26–28] and HyPer and derivatives.[29,30] These biosensors undergo ratiometric fluorescence changes that are monitored with flow cytometry, fluorescence microscopy, or fluorescence plate readers. We have previously used two of these reporters in fission yeast: roGFP2-Tpx1.C169S[21] and HyPer7.[30,31] Both probes are exquisitely sensitive to sense moderate fluctuations of H_2O_2, and while roGFP2-Tpx1.C169S is ~5 times more sensitive, HyPer7 has been successfully expressed not only in the cytosol but also in the mitochondrial matrix.[31] Using the basal oxidation level of these biosensors as a proxy to calculate relative H_2O_2 concentrations, we determined that the peroxide concentration in the matrix of fission yeast is significantly higher than in the cytosol,[31] ~150 nM, similar to the concentration established before in higher eukaryotes.[32] It is widely recognized that the steady-state levels of cytosolic H_2O_2 in both eukaryotic and prokaryotic cells is in the low nanomolar range.[13,33,34] This steep gradient between the matrix and the cytosol is caused by cytosolic scavenging by Tpx1, since, in cells lacking this cytosolic peroxiredoxin, this matrix-to-cytosol peroxide gradient disappears with a concomitant increase of H_2O_2 in both compartments,[31] reaching toxic peroxide values around 0.3 μM.[22]

While the participation of high levels of mitochondrial ROSs in toxicity is well established,[35] it is still under debate whether H_2O_2 emanating from the mitochondria can reach the nucleus[36–38] and/or engage in cytosolic signaling cascades to regulate cell physiology.[39,40] Here, we aimed to study how far an initial burst of H_2O_2 can reach across cellular membranes in intact cells, using genetically encoded tools to trigger ROS fluxes, to control them with scavengers, and to monitor their spreading with biosensors. We used two main H_2O_2 sources: from the extracellular milieu, by the addition of H_2O_2 to the media; and emanating from the matrix from ectopically expressed mitochondrially targeted D-amino acid oxidases (DAOs), which generate H_2O_2 as a product from D-amino acids. By expressing the H_2O_2 biosensor HyPer7 in different compartments, we monitored peroxide waves and measured permeability gradients across membranes from both extracellular and matrix origins. We unambiguously determined that antioxidant cascades driven by the transcription factors Atf1 and Pap1 can be activated by H_2O_2 of mitochondrial origin and that artificially scavenging these peroxide fluxes with the expression of mitochondrial H_2O_2 scavengers, Ctt1 (catalase) or Tpx1 (peroxiredoxin), avoided these signaling events and negatively contributed to cell fitness.

RESULTS

Measurement of peroxide gradients across membranes in response to extracellular H_2O_2

We measured how far H_2O_2 fluxes can reach when the initial burst starts in the extracellular milieu. We expressed HyPer7 in four different subcellular compartments: the mitochondrial matrix, the mitochondrial intermembrane space (IMS), the cytosol, and the nucleus. Of note, our original HyPer7 probe[31] was located at both the cytosol and the nucleus; by adding a nuclear localization signal (NLS) or a bulky protein (maltose-binding protein [MBP]) at the N-terminal domain of the biosensor, we accomplished exclusive localization at the nucleus or the cytosol, respectively (Figure S1A). We decided to discard a nuclear-export signal (NES)-tagged HyPer7: it triggered cytosolic localization of the biosensor but probably affected its functionality since it sensed H_2O_2 less on average than untagged HyPer7 (Figure S1B). We added different concentrations of peroxides to the media of cells expressing each one of the five reporters (Figure 1A) and measured probe oxidation in the different compartments. The basal levels of oxidation of HyPer7 (OxD_0) in the matrix were ~40%, as previously reported,[31] while the OxD_0 levels of IMS-HyPer7 were ~20%, suggesting higher levels of peroxides in both compartments than in the cytosol (with an OxD_0 of 0). For any given concentration of peroxide and time, the levels of probe oxidation changed depending on the localization of the probe. As shown as an example in Figure 1B for the response to 100-50-25 μM H_2O_2 at 5 min after treatment, maximal oxidation was observed for cytosolic MBP-HyPer7, while the lower oxidation values corresponded to MTS-HyPer7; similar levels were observed for IMS-HyPer7 and MTS-HyPer7. We averaged the oxidation values of each probe in the range of 25 to 50 μM peroxides and compared them with those of cytosolic MBP-HyPer7. Based on our experimental data, which indicate that the concentration of H_2O_2 decreases by 300-fold from the extracellular milieu to the cytosol due to both the membrane permeability gradient and Tpx1-mediated scavenging,[22] we now propose additional relative gradients across membranes. Specifically, the previously calculated 300:1 ratio from the extracellular milieu to the intracellular space is further amplified to reach other compartments, with increases of 3-fold (cytosol to nucleus), 5-fold (cytosol to IMS), and 6-fold (cytosol to matrix), as indicated in Figure 1C.

Initiating intracellular H_2O_2 fluxes by expression of DAO from *Rhodotorula gracilis* in fission yeast

Originally described by Krebs in 1935,[41] DAO is a flavin adenine dinucleotide (FAD)-containing flavoenzyme that catalyzes the

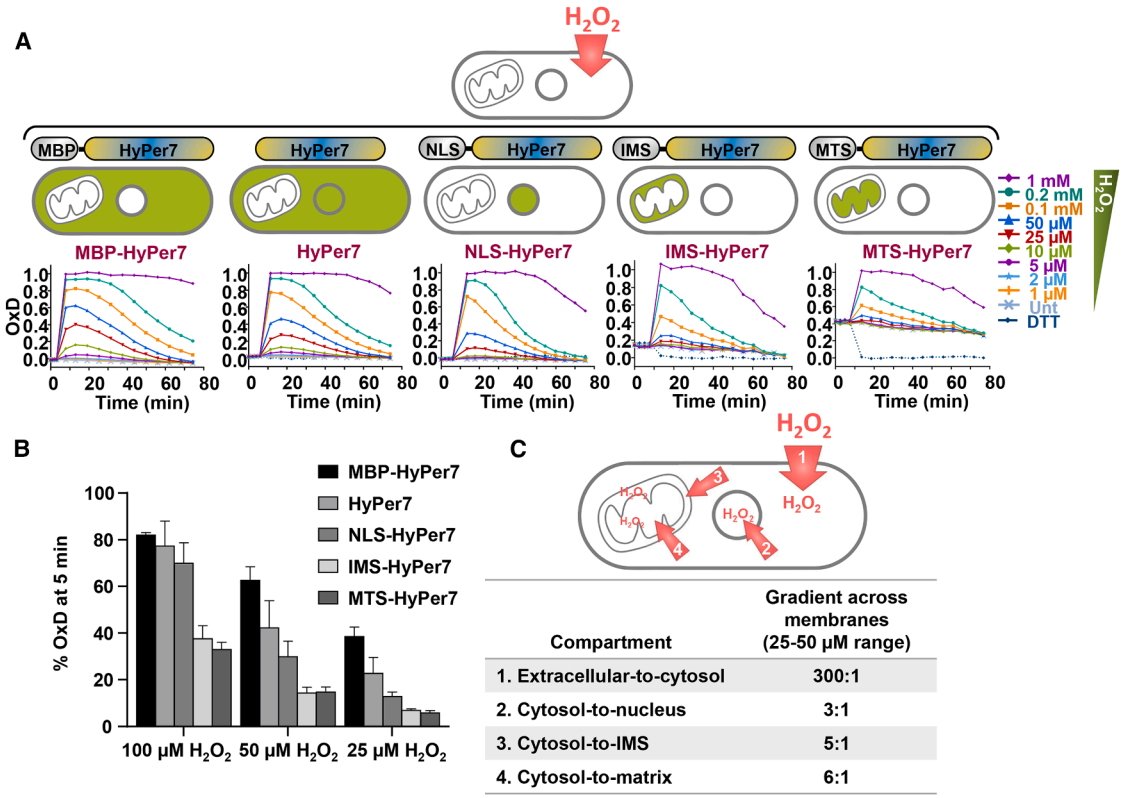

Compartment	Gradient across membranes (25-50 µM range)
1. Extracellular-to-cytosol	300:1
2. Cytosol-to-nucleus	3:1
3. Cytosol-to-IMS	5:1
4. Cytosol-to-matrix	6:1

Figure 1. Measurement of peroxide gradients across membranes in response to extracellular H_2O_2

(A) Strain HM123 (WT) was transformed with plasmids p862 (coding for MBP-HyPer7), p728 (HyPer7), p840 (NLS-HyPer7), p836 (IMS-HyPer7), and p730 (MTS-HyPer7); the subcellular localization of the biosensors is indicated in green. Fluorescence of the probes was recorded in 96-well imaging plates at 30°C with shaking. Measurements were taken before (untreated [Unt]) and after adding the indicated concentrations of H_2O_2 to MM cultures at an optical density 600 (OD_{600}) of 1. The degree of probe oxidation (per 1) is shown on the *y* axis (OxD), with the values obtained after treatment with 1 mM H_2O_2 and dithiothreitol (DTT) representing complete (1) and no (0) probe oxidation, respectively. For each panel, data from three biological replicates are shown, with error bars displayed in Figure S1.

(B) Bar graph showing average percentage of oxidation from A. % OxD was calculated as the average of biosensor oxidation (OxD) 5 min after treatment with the indicated H_2O_2 concentrations. 0%, value of OxD in untreated (no H_2O_2) conditions; 100%, value of OxD upon 1 mM H_2O_2 (OxD of 1 for all biosensors). Average data from three biological replicates with error bars (standard deviation) are shown.

(C) Calculated gradients from extracellularly applied H_2O_2. The relative gradients were calculated using data from (B) for treatments of 25 and 50 µM H_2O_2. See also Figure S1.

oxidative deamination of D-amino acids to give α-keto acids and ammonia; reduced FAD reoxidizes then from oxygen to H_2O_2[42] (Figure 2A). Ectopically expressed DAO can serve as a genetically encoded producer of H_2O_2 in a D-amino acid-dependent manner, as shown before in mammalian cells.[43,44] In particular, the red yeast *R. gracilis*'s DAO (*Rg*DAO) has been expressed in different cell types to initiate redox events in specific locations. We expressed *Rg*DAO in the cytosol of fission yeast and monitored H_2O_2 production with the aid of the sensitive biosensor roGFP2-Tpx1.C169S (Figure 2B). As shown in Figures 2C and S2A, addition of D-alanine (D-Ala) or the non-proteinogenic D-norvaline (D-Nor) caused a concentration-dependent oxidation of the biosensor. High concentrations of D-serine induced a small but significant oxidation of the biosensor, while D-proline, or L-Ala, L-serine or L-Nor did not (Figure 2D).

We then analyzed the levels of probe oxidation co-expressing *Rg*DAO in the same compartment as the biosensor HyPer7.[31] The degree of oxidation of HyPer7 was not as dramatic as that of roGFP2-Tpx1.C169S (compare the graphs in Figures 2C–2E and S2B), as expected from the different sensitivity to peroxides of both biosensors. We determined the oxidation of MTS-HyPer7 in the matrix upon addition of D-Ala or D-Nor when MTS-*Rg*DAO was co-expressed at the matrix. The subcellular localization of MTS-*Rg*DAO and other ectopically expressed proteins in this study was confirmed by protein-extract fractionation (Figure S3A) and fluorescence microscopy (Figure S3B). As shown in Figures 2F and S2C, expression of MTS-*Rg*DAO in the matrix allowed H_2O_2 production, which acted locally and oxidized MTS-Hyper7 and induced stronger oxidation of the probe than when both *Rg*DAO and HyPer7 were co-expressed in the cytosol. This difference was probably caused by the absence of strong peroxide scavengers in the matrix and by the role in the cytosol of the peroxiredoxin Tpx1.[31]

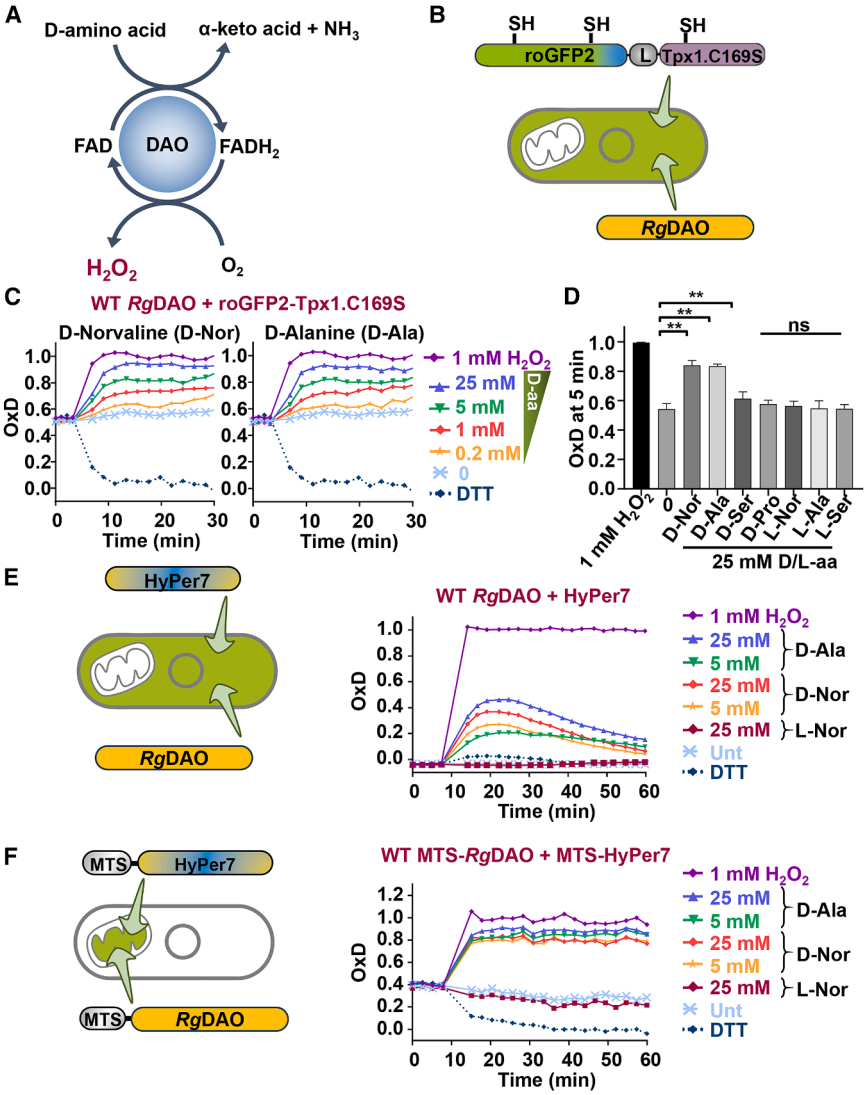

Figure 2. Initiating intracellular H_2O_2 fluxes by expression of D-amino acid oxidase from *R. gracilis*

(A) The enzymatic reaction of D-amino acid oxidases (DAOs).

(B) The experimental setup for (C) and (D) in which we co-express the cytosolic biosensor roGFP2-Tpx1.C169S with the cytosolic H_2O_2 producer *Rg*DAO.

(C) Strain JM25 (expressing *Rg*DAO) transformed with plasmid p407.C169S (roGFP2-Tpx1.C169S) was treated as described in Figure 1A with the indicated concentrations of D-norvaline (D-Nor) or D-alanine (D-Ala). For each panel, data from three biological replicates are shown, with error bars displayed in Figure S2.

(D) Strain as in (C) was treated with 25 mM of the indicated D- and L-amino acids. % OxD, calculated as in Figure 1B, is represented. Data from three biological replicates and error bars are shown. Significant differences between treatments were determined by two-sided *t* test (**$p \leq 0.01$; ns, not significant).

(E and F) Strain JM25 (expressing *Rg*DAO) (E) and JM27 (expressing MTS-*Rg*DAO) (F) were transformed with plasmid p728 (for expression of HyPer7) or with p730 (for expression of MTS-HyPer7). Experiments were performed as indicated in Figure 1A treating cells with the indicated concentrations of D/L-amino acids. For each strain, average data from three biological replicates are shown.

Figures with error bars are displayed in Figure S2. See also Figures S2 and S3.

Use of *S. pombe* D-amino acid oxidase Dao1 as a genetically encoded H_2O_2 generator to induce nanomolar increases in peroxide levels upon D-Nor addition

S. pombe encodes a DAO protein, Dao1, of 348 amino acids (Figure 3A). It has been proposed that, in other yeasts, some family members are involved in metabolism to mediate the efficient utilization of D-amino acids for cell growth, and they normally display peroxisomal localization. The role of DAO enzymes in higher organisms is not entirely clear and may be related to detoxification, regulation of neuromodulators in the human brain, or even antimicrobial roles in the gastrointestinal system.[42,45] No role has been assigned to the fission yeast Dao1.

We first tested whether addition of D-amino acids to cultures of wild-type (WT) *S. pombe* expressing the biosensor roGFP2-Tpx1.C169S could trigger its oxidation (Figure S4A). A mild but significant oxidation of the probe was detected upon addition of high concentrations of D-Nor (5 or 25 mM) to the growing medium, and this oxidation was not observed in cells lacking Dao1. To confirm that this oxidation was driven by H_2O_2 generated during the reaction of D-Nor with Dao1, we used a Δ*tpx1* background: the absence of this essential peroxide scavenger would maximize the interaction of the secondary product H_2O_2 with the biosensor. As shown in Figure S4B, probe oxidation was significantly higher in strain Δ*tpx1* than in the WT background upon D-Nor addition.

We expressed *S. pombe*'s Dao1 from the strong and constitutive *sty1* promoter and measured its H_2O_2-generation activity using the biosensor roGFP2-Tpx1.C169S (Figure 3B). Dao1 was able to generate H_2O_2 with D-amino acids but not with L-amino acids, similar to *Rg*DAO (compare Figure 3B for Dao1 with Figure 2D for *Rg*DAO). Dao1 had been previously overexpressed in *Escherichia coli*, and the activity of crude extracts assayed; in concordance with our *in vivo* data, recombinant Dao1 displayed activity against neutral and basic D-amino acids such as D-Ala or D-Ser, and there was no activity against L-Ala.[46] To simplify data interpretation, from this point forward, D-Nor will be used to induce H_2O_2 production by *Rg*DAO or Dao1, while L-Nor will serve as a negative control.

By co-expressing the cytosolic biosensor HyPer7 with either cytosolic (Figures 3C and S4C) or mitochondrial (Figures 3D

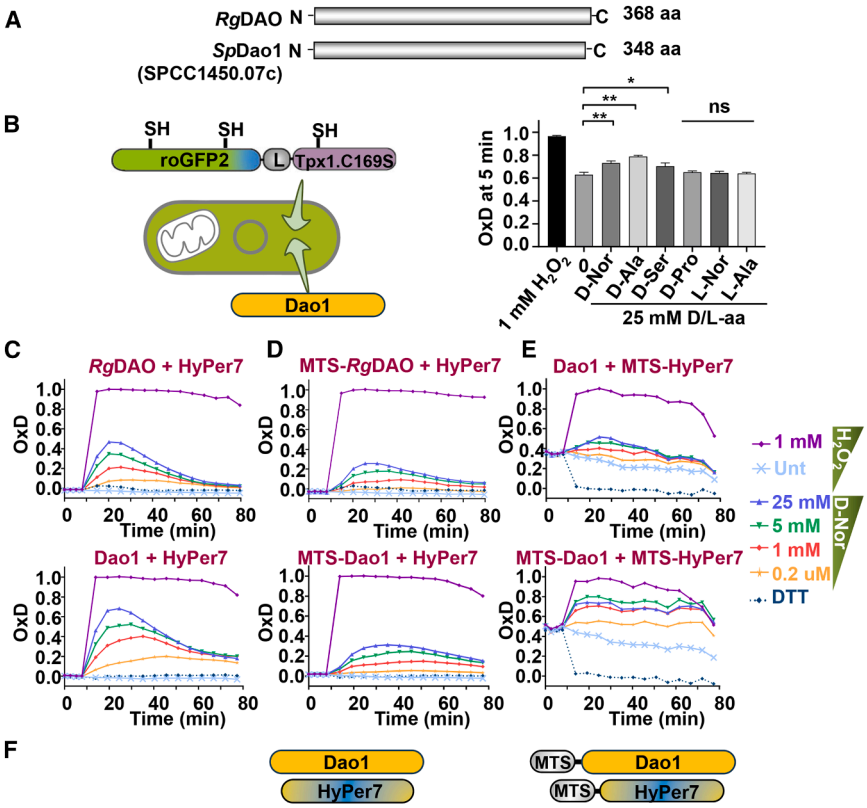

D-Nor (concentration in media)	Dao1 (in cytosol)		MTS-Dao1 (in matrix)	
	Equivalence with H_2O_2 in media	Increase of H_2O_2 in cytosol	Equivalence with H_2O_2 in media	Increase of H_2O_2 in matrix
0.2 mM	~25 μM	~80 nM	~80 μM	~40 nM
1 mM	~50 μM	~170 nM	~150 μM	~80 nM
5 mM	~70 μM	~225 nM	~190 μM	~100 nM
25 mM	~90 μM	~290 nM	>400 μM	>200 nM

Figure 3. Use of *S. pombe* D-amino acid oxidase Dao1 as a genetically encoded H_2O_2 generator

(A) Scheme of the *R. gracilis* (*Rg*DAO) and *S. pombe* (Dao1) DAO enzymes. Number of amino acids is indicated. The reference number for Dao1 is shown.

(B) Left: the experimental setup for co-expressing the biosensor roGFP2-Tpx1.C169S and the *S. pombe* Dao1. Strain LC128 (expressing Dao1) was transformed with plasmid p407.C169S (roGFP2-Tpx1.C169S). Bars were done as described in Figure 1B. Data from triplicates and error bars are shown. Significant differences between treatments were determined by two-sided *t* test (*$p \leq 0.05$; **$p \leq 0.01$; ns, not significant).

(C–E) The degree of probe oxidation of HyPer7 (C and D) or MTS-HyPer7 (E) was determined as in Figure 1A treating with the indicated concentrations of D-Nor. (C and D) Strains JM25 (expressing RgDAO), LC128 (expressing Dao1) (C), JM27 (expressing MTS-RgDAO), LC99 (expressing MTS-Dao1) (D), were transformed with plasmid p728, coding for HyPer7. (E) Strains LC128 (Dao1) and LC99 (MTS-Dao1) were transformed with plasmid p730, coding for MTS-HyPer7. For each strain or panel, average data from three biological replicates are shown. Figures with error bars are displayed in Figure S3.

(F) Equivalence of H_2O_2 production to D-Nor concentrations added to the media produced by cytosolic Dao1 or mitochondrial MTS-Dao1. Probe oxidation (OxD) values 5 min post treatment with H_2O_2 (from Figure 1A) or D-Nor (from Figures 3C and 3E, considering only Dao1 or MTS-Dao1 panels) were normalized to percentage (% OxD) as in Figure 1B. Oxidation percentages were compared with biosensor oxidation by extracellular H_2O_2 obtained in Figure 1A to estimate equivalence, and compartmental H_2O_2 increases were calculated using gradients from Figure 1C. For treatments with 25 mM D-Nor in MTS-Dao1-expressing cells, biosensor saturation prevented precise quantification; the intracellular H_2O_2 concentrations were estimated to be substantially higher than those induced by 5 mM D-Nor; see text for details.

See also Figure S4.

and S4D) *Rg*DAO or Dao1, we confirmed that both DAOs generated similar concentrations of H_2O_2 in both compartments upon the addition of D-Nor to the medium.

We also used MTS-HyPer7 to monitor peroxide fluctuations from Dao1 expressed in the mitochondria or in the cytosol. As shown in Figure 3E (lower panel) and Figure S4E, MTS-Dao1 induced substantial amounts of mitochondrial peroxides with 0.2 to 25 mM D-Nor in the medium; H_2O_2 produced by cytosolic Dao1 also reached the matrix, as demonstrated with MTS-HyPer7 (Figure 3E, upper panel).

We chose to continue our studies with ectopically expressed *S. pombe* Dao1, using four concentrations of D-Nor (0.2–25 mM), spanning two orders of magnitude. To estimate the increase in H_2O_2 caused by D-Nor addition in cells expressing Dao1 or MTS-Dao1, we measured the maximal oxidation of the biosensors (OxD) following D-Nor addition, and compared it with the effect of extracellular H_2O_2 applied to the medium. Thus, we applied D-Nor to a strain co-expressing Dao1 and HyPer7 to estimate the increase in H_2O_2 in the cytosol or to a strain co-expressing MTS-Dao1 and MTS-HyPer7 to assess the rise in peroxide levels within the mitochondrial matrix. Using the experimentally determined peroxide gradients from the extracellular milieu to the cytosol and further into the mitochondrial matrix (Figure 1), we correlated HyPer7 and MTS-HyPer7 oxidation values (OxD) with H_2O_2 concentrations (Figure S4F), with the results shown in Figure 3F. For example, in the strain co-expressing MTS-Dao1 and MTS-HyPer7, the addition of 1 mM D-Nor triggered biosensor oxidation comparable to that induced by ~150 μM extracellular H_2O_2. Given the 300:1 gradient from the extracellular medium to the cytosol and the 6:1 gradient from the cytosol to the matrix, this corresponds to an estimated increase of ~80 nM H_2O_2 in the matrix. The biosensor appeared to become saturated at higher concentrations of D-Nor; we estimated that treatment with 25 mM D-Nor in

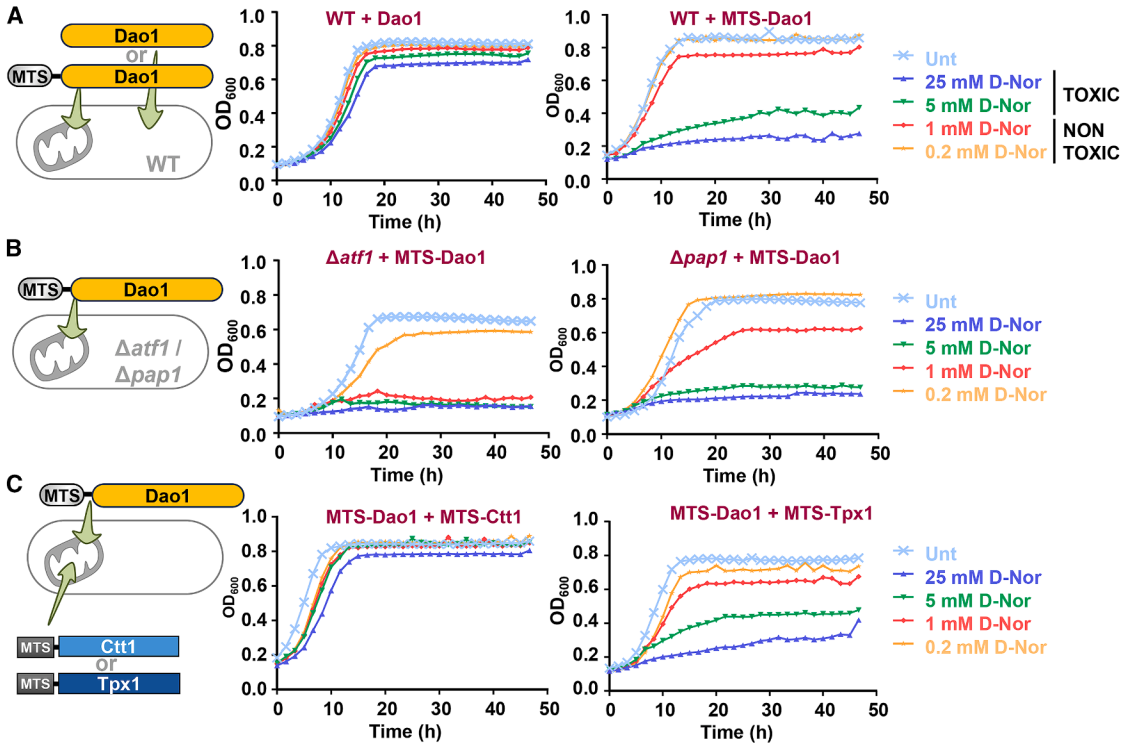

Figure 4. High D-Nor concentrations caused growth inhibition to MTS-Dao1-expressing cells in a H_2O_2-dependent manner

Growth curves of strains LC153 (WT expressing Dao1) and LC154 (WT expressing MTS-Dao1) (A), LC124 (Δ*atf1* expressing MTS-Dao1) and LC162 (Δ*pap1* expressing MTS-Dao1) (B), MFC11 (WT expressing MTS-Dao1 and MTS-Ctt1) and MFC8 (WT expressing MTS-Dao1 and MTS-Tpx1) (C). Strains were grown in MM to mid-logarithmic phase, then diluted to an OD_{600} of 0.1, and growth was monitored by recording OD_{600} at the indicated times (in hours) in the presence or not of the indicated treatments for a period of 48 h at 30°C with continuous shaking in 96-well plates. For each strain, average data from three biological replicates are shown.

See also Figure S5.

MTS-Dao1-expressing cells increased intra-matrix peroxide levels over 200 nM (Figure 3F). Thus, we conclude that adding different concentrations of D-Nor to cells expressing Dao1 or MTS-Dao1 can induce H_2O_2 increases in the range of 40–300 nM.

H_2O_2 produced in the matrix by MTS-Dao1 in response to high D-Nor concentrations triggered mitochondrial toxicity

The use of DAO enzymes as chemogenetic tools to trigger H_2O_2 production involves the addition of D-amino acids to the media, and this could affect other processes linked or not to the ectopic expression of the enzymes. We noticed that high concentrations of D-amino acids did not affect the growth of WT or Δ*dao1* strains (Figure S5A), but addition of L-Nor did (Figure S5B). The toxicity caused by 25 mM L-Nor was not dependent on the ectopic expression of Dao1 and was not altered by deletion of the *pap1* or *atf1* genes or overexpression of peroxide scavengers, indicating that this toxicity is not related to oxidative stress (Figure S5B). In fact, L-Nor did not oxidized the MTS-HyPer7 biosensor even at high concentrations (Figure S5C).

To monitor the effect of different concentrations of D-Nor, ranging again from 0.2 to 25 mM and triggering endogenous H_2O_2 production, in the growth of cells expressing Dao1 or MTS-Dao1, we recorded the growth curves upon addition of the D-amino acids to minimal-medium cultures. As shown in Figure 4A, D-Nor barely affected the growth of Dao1-expressing cells (left graph), while 5 and 25 mM D-Nor strongly inhibited the growth of cells expressing MTS-Dao1 (right graph). Other D-amino acids added at 25 mM also affected the growth of MTS-Dao1-expressing (but not Dao1-expressing) cells (Figure S5D). Of note, addition of D-Nor to rich-medium cultures did not affect the growth of these strains, probably due to the inhibition of amino acid internalization (Figure S5E). This toxic effect, proportional to the concentration of D-Nor added to the medium, was also observed when MTS-Dao1 was expressed in *Saccharomyces cerevisiae* (Figure S5F).

To test whether the toxicity of D-Nor to MTS-Dao1-expressing cells was specifically caused by increases of H_2O_2, we monitored the effect of deleting *atf1* or *pap1*. As shown in Figure 4B, lack of Pap1 (right panel) and specially of Atf1 (left panel) severely enhanced the toxicity of D-Nor to cells expressing MTS-Dao1. On the contrary, co-expression of MTS-Ctt1 fully abolished toxicity of D-Nor addition (Figure 4C), suggesting that the elevated levels of H_2O_2 upon addition of 5 or 25 mM D-Nor to cells expressing MTS-Dao1 was causing severe mitochondrial

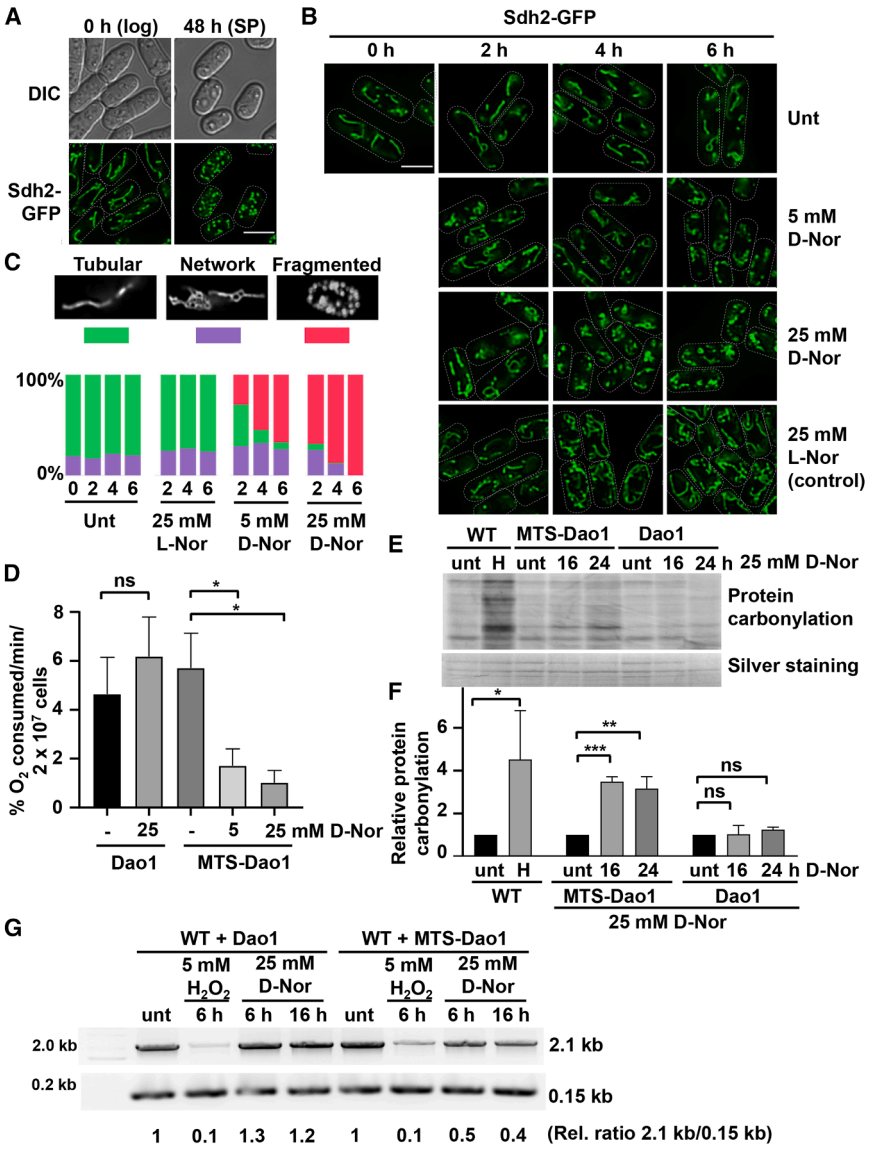

Figure 5. H_2O_2 produced in the matrix by MTS-Dao1 at high D-Nor levels triggered mitochondrial toxicity

(A) Fluorescence micrographies of strain LC164 expressing the mitochondrial marker Sdh2-GFP at the logarithmic phase (log) and 48 h later at stationary phase (SP). The same cells under differential interference contrast (DIC) optics and red fluorescence are shown. Scale bar, 5 μM.

(B) Fluorescence micrographs of strain of Figure 5A. Cells were treated with the indicated concentrations of amino acids, and samples were collected and analyzed every 2 h. Scale bar, 5 μM.

(C) Classification of mitochondrial morphology phenotypes upon amino acid treatment. Mitochondria from (B) were manually classified as tubular, network, or fragmented. Bar graphs represent the % of cells from each category during the indicated time points and treatments. At least 50 cells were quantified for each treatment and strain.

(D) Oxygen consumption of strains LC153 (expressing Dao1) and LC154 (expressing MTS-Dao1). Cells were grown in MM and treated or not for 16 h with the indicated concentrations of D-Nor. Data from three biological replicates and error bars are shown. Significant differences between deletion strains and WT were determined by two-sided *t* test (*$p \leq 0.05$; ns, not significative).

(E) Protein carbonylation assay. Strain 972 (WT) was treated as control with 5 mM H_2O_2 for 4 h (H). Strains from (D) were treated for 16 or 24 h with 25 mM D-Nor. After protein extraction, carbonyls were derivatized with fluorescein thiosemicarbazide for fluorescent detection. Total protein concentration was detected by silver staining.

(F) Quantification of panels of Figure 5E. After total quantification, each treatment was corrected to protein concentration and then normalized to each strain untreated. Average data from three biological replicates and error bars are shown. Significant differences between deletion strains and WT were determined by two-sided *t* test (*$p \leq 0.05$; **$p \leq 0.01$; ***$p \leq 0.001$; ns, not significant).

(G) Mitochondrial DNA damage. Total DNA from cultures of strains as in (D), treated or not with toxic doses of H_2O_2 or D-Nor for the times indicated, was obtained and used as template for the amplification of large (2.1 kb) or small (0.15 kb) fragments of mitochondrial DNA. The relative ratios of 2.1/0.15 kb are indicated and are indicative of template damage. See STAR Methods for details.

See also Figure S6.

damage that could be prevented with the peroxide scavenger Ctt1. Expression of the peroxiredoxin MTS-Tpx1 only had a mild protective effect, probably due to its inactivation by high concentrations of H_2O_2.[47]

Mitochondrial morphology is an indicator of cellular fitness. It changes with chronological aging, shifting from a tubular morphology during active growth to fragmented mitochondria at the stationary phase and in mutants with defective mitochondrial homeostasis,[48] as observed using the complex II tagged subunit Sdh2-GFP as a reporter (Figure 5A). We monitored the effects on mitochondrial morphology of toxic concentrations of D-Nor to MTS-Dao1-expressing cells (Figure 5B). Toxic concentrations of D-Nor, but not of the control L-Nor, to cells expressing MTS-Dao1 and Sdh2-GFP triggered a dose-dependent mitochondrial fragmentation 2 or 4 h after D-amino acid addition (Figure 5B; quantified in Figure 5C). Cells expressing cytosolic Dao1 did not suffer mitochondrial morphological changes upon addition of D-Nor (Figure S6A), confirming the lack of toxicity of enhanced cytosolic H_2O_2 levels (Figure 4A). These changes in mitochondrial morphology in cells expressing MTS-Dao1 preceded a decrease in oxygen consumption, demonstrating an impairment of mitochondrial functions (Figure 5D). We also determined a global increase in total protein carbonylation (Figures 5E; quantified in Figure 5F) and of mitochondrial DNA damage (Figure 5G) in cells expressing MTS-Dao1 but not Dao1 upon addition of 25 mM D-Nor. No indications of nuclear

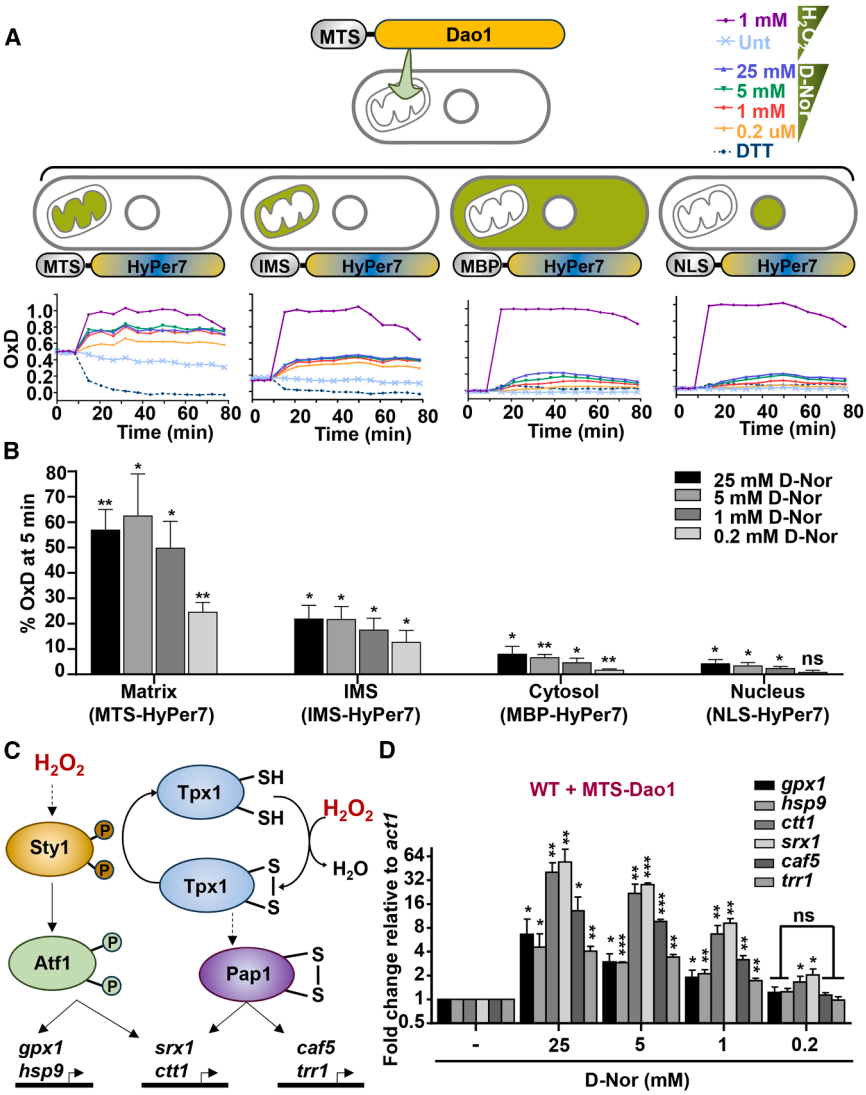

Figure 6. H_2O_2 gradients originating in the mitochondrial matrix propagated to the cytosol and nucleus

(A) Strain LC99 (expressing MTS-Dao1) was transformed with the plasmids p730 (coding for MTS-HyPer7), p836 (IMS-HyPer7), p862 (MBP-HyPer7), or p840 (NLS-HyPer7) and their localization is indicated in green in the image. Experiments were performed as described in Figure 1A using the indicated concentrations of D-Nor. For each strain, average data from three biological replicates are shown with error bars displayed in Figure S7.

(B) Bar graph from (A) depicting % of probe oxidation as done in Figure 1B. Data from biological triplicates with error bars are shown. Significant differences between treatments were determined by two-sided *t* test (*$p \leq 0.05$; **$p \leq 0.01$; ns, not significant).

(C) Scheme depicting the two anti- H_2O_2 response pathways of *S. pombe*. On the left, the mitogen-activated protein (MAP) kinase Sty1 become activated upon H_2O_2 treatment, activating the transcription factor Atf1. On the right, the peroxiredoxin Tpx1 acts as a scavenger until it accumulates in the oxidized form and activates the transcription factor Pap1. Genes upregulated by each one of these pathways include *gpx1* and *hps9* (Sty1-Atf1 dependent), *caf5* and *trr1* (Tpx1-Pap1 dependent), and *srx1* and *ctt1* (activated by both pathways).

(D) Expression of stress gene mRNA was analyzed by qPCR upon treatment with the indicated concentration of D-Nor for 20 min. Total RNA of strain LC155 (expressing MTS-Dao1) was obtained and quantified by qPCR. *act1* was used as a control. For each strain, average data from three biological replicates with error bars are shown. Significant differences between treatments were determined by two-sided *t* test (*$p \leq 0.05$; **$p \leq 0.01$; ***$p \leq 0.001$; ns, not significant).

See also Figure S7.

DNA damage were observed in Dao1- or MTS-Dao1-expressing cells upon D-Nor addition (Figure S6B). These results suggest that increases of ~100–200 nM concentrations of mitochondrial, but not cytosolic, H_2O_2 can severely affect cell viability through mitochondrial oxidative damage.

H_2O_2 gradients originating in the mitochondrial matrix can propagate to the cytosol and nucleus

Using MTS-Dao1 as a genetic tool to initiate H_2O_2 bursts from the matrix, we measured how far the peroxide wave could propagate. To do this, we expressed MTS-Dao1 alongside each of the four HyPer7 derivatives located at the matrix, the IMS, the cytosol, and the nucleus of fission yeast and added 0.2 to 25 mM D-Nor to the medium (Figures 6A and S7A). For a given concentration of D-Nor, maximal probe oxidation was higher in the matrix that in the IMS, the cytosol, or the nucleus (Figure 6B). In fact, oxidation of NLS-HyPer7 was barely detected, implying that H_2O_2 fluxes emanating from the mitochondria reach the nucleus but are unlikely to trigger toxicity, as recently demonstrated in human cells using a similar chemogenetic approach.[36] We also demonstrated that these mitochondria-to-cytosol peroxide fluxes could be totally or partially eliminated by co-expression of MTS-Dao1 with MTS-Ctt1 or MTS-Tpx1, respectively (Figure S7B).

In contrast, we hypothesized that the concentrations of H_2O_2 originating from the mitochondria in MTS-Dao1-expressing cells could be high enough to initiate signaling events in the cytosol. In fission yeast, two pathways respond to H_2O_2 fluctuations: the Tpx1-Pap1 pathway, which responds to moderate increases of peroxides, and the Sty1-Atf1 pathway which is activated by higher levels of the oxidant and also senses many other types of stressors[49,50] (Figure 6C). We did not detect activation of these cascades in MTS-Dao1-expressing cells upon D-Nor addition by western blot analysis (i.e., phosphorylation of Sty1 of Atf1, or oxidation of Tpx1 or Pap1), probably due to lack of sensitivity of the assay (Figure S7C). The activated transcription

factors Atf1 and Pap1 upregulate the expression of some specific and common genes.[51] We tested by quantitative polymerase chain reaction (qPCR) the expression of these genes in cells expressing MTS-Dao1 upon addition of D-Nor to demonstrate that they were all induced to different extents (Figure 6D). We concluded that MTS-Dao1 can initiate H_2O_2 fluxes that can activate cytosolic cascades and change the cellular gene expression program.

Activation of antioxidant cascades by mitochondria-derived, non-toxic H_2O_2 fluxes promoted stress adaptation and lifespan extension

We investigated whether non-toxic peroxide fluxes generated at the mitochondria upon 0.2 or 1 mM D-Nor addition to MTS-Dao1-expressing cell cultures could positively influence cell physiology. We first confirmed that the continuous production of H_2O_2 using 1 mM D-Nor did not negatively affect cell growth: (1) the proliferative potential of cell cultures, using the duplication time of MTS-Dao1-expressing cells before and after the addition of 1 mM D-Nor, barely moved from 3 to 3.7 h (Figure 4A); (2) the oxygen-consumption values of logarithmic- or stationary-phase MTS-Dao1-expressing cultures was unaffected by the addition of 1 mM D-Nor; and (3) no indication of accumulated DNA damage 24 h after addition of 1 mM D-Nor were observed using phosphorylation of histone H2B as a hallmark (Figure S6B).

Regarding H_2O_2-mediated gene expression, as shown in Figure 6C, the transcription factors Pap1 and Atf1 can induce anti-stress genes once activated by extracellular peroxides. We first confirmed that these transcription factors mediated stress gene activation upon 1 and 0.2 mM D-Nor in MTS-Dao1-expressing cells (Figure 7A). Indeed, Atf1 was very important for the activation of *gpx1* or *hsp9*, while, in the absence of Pap1, expression of *ctt1*, *caf5*, *srx1*, or *trr1* was limited.

Once established that non-toxic, moderate concentrations of mitochondrial H_2O_2 were capable of triggering matrix-to-cytosol redox communication, we searched for physiological consequences of this signal transduction. Stress adaptation is a process by which a cell or organism can gain strength or fitness from previous exposure to a non-toxic dose of the stressor. Thus, it has been previously demonstrated that high doses of extracellular peroxides can dramatically decrease survival of *S. pombe* cell cultures, while pre-treatments with non-toxic doses of H_2O_2 trigger an adaptive response resulting in population survival.[52] We tested whether killing by a toxic dose of H_2O_2 could be attenuated by previous mitochondrial fluxes of H_2O_2 emanating from the mitochondrial matrix. Thus, we compared survival percentages of cell cultures of a strain expressing or not MTS-Dao1, treated or not with 50 mM H_2O_2, which had been or not pre-treated with 1 mM D-Nor or with low concentrations of H_2O_2 as a control (Figure 7B). As shown in Figure 7C (and quantified in Figure 7D), the colony-forming units of *S. pombe* cultures decreased by 2–3 orders of magnitude upon treatment for 60 min with 50 mM H_2O_2. On the contrary, pre-treatment with 1 mM D-Nor for 2 h prior to the toxic threat largely decreased the toxic effects to the same extent as cells pre-treated with 0.5 mM H_2O_2. The treatment with D-Nor had no protective effect when added to WT cells not expressing mitochondrially tagged MTS-Dao1 (“WT C” in Figure 7C). As controls, cells lacking the transcription factor Atf1 or Pap1, and therefore avoiding the activation of the stress genes (Figure 7A), largely reduced the adaptation effect of D-Nor or H_2O_2 on MTS-Dao1-expressing cells (Figures S8A–S8C).

We tested whether the scavengers MTS-Ctt1 or MTS-Tpx1 could block signal transduction when co-expressed with MTS-Dao1 (Figure S8A). Expression of MTS-Ctt1 or MTS-Tpx1 fully or partially, respectively, decreased the toxicity of 50 mM H_2O_2 on cultures, confirming their peroxide-scavenging capacity (compare “B” in Figure S8B, quantified in Figure S8C). Nevertheless, at least for MTS-Tpx1-expressing cells, no beneficial effects of 1 mM D-Nor could be observed (“C” in Figure S8C, right panel), suggesting that mitochondrial H_2O_2 scavenging would abolish redox responses initiated from peroxides of mitochondrial origin. In fact, activation of stress genes in MTS-Dao1-expressing cells was largely attenuated 20 min (Figure S8D) or 30 min (Figure S8E) after D-Nor addition in cells expressing MTS-Ctt1 or MTS-Tpx1, respectively.

To test whether the continuous generation of moderate waves of mitochondrial H_2O_2 could have beneficial long-term effects on longevity, we monitored CLS to MTS-Dao1-expressing cell cultures in minimal medium treated or not from the logarithmic phase with 1 mM D-Nor (see STAR Methods), by testing viability 8 or 10 days after reaching stationary phase (Figure 7E). As a control, we used the long-lived mutant Δ*pka1*.[15] As shown in Figure 7F (and quantified in Figure 7G), the survival at day 8 of stationary phase was ~1–2 orders of magnitude lower for WT cells than for Δ*pka1*, and MTS-Dao1-expressing cultures treated with D-Nor displayed a survival similar to that of the long-lived mutant Δ*pka1*; D-Nor had no beneficial effects on WT cells not expressing MTS-Dao1. The mitochondrial H_2O_2 fluxes initiated upon D-Nor in MTS-Dao1-expressing cells did not promote longevity in cells depleted of Atf1 or Pap1 (Figures S9A, S9B, and S9C). Beneficial effects of D-Nor on CLS were also blocked by over-expressing scavengers at the mitochondrial matrix (Figures S9A–S9D and S9E). In conclusion, moderate mitochondrial peroxide fluxes have beneficial effects on cell physiology, such as inducing adaptation to toxic stressors or promoting longer lifespan.

DISCUSSION

The molecular mechanisms underlying cell fitness and aging are conserved across most organisms. We use CLS, defined as the survival of non-proliferating cells, as an indicator of health and longevity in fission yeast. Calorie restriction is widely regarded as one of the most common interventions to promote both cell fitness and extended lifespan. Its effects are linked to the activation or inhibition of nutrient-sensing pathways, stimulation of mitochondrial metabolism, ROS production, and the activation of stress-regulated kinases. However, demonstrating each step of this cascade has proved to be controversial. To address this, we have developed a combined approach to demonstrate the role of mitochondrial-produced H_2O_2 in promoting CLS through the activation of anti-stress pathways. The redox toolkit used here includes H_2O_2 generators, scavengers, and biosensors.

Mitochondria are likely the primary source of ROSs, and we were particularly interested in determining whether H_2O_2 of

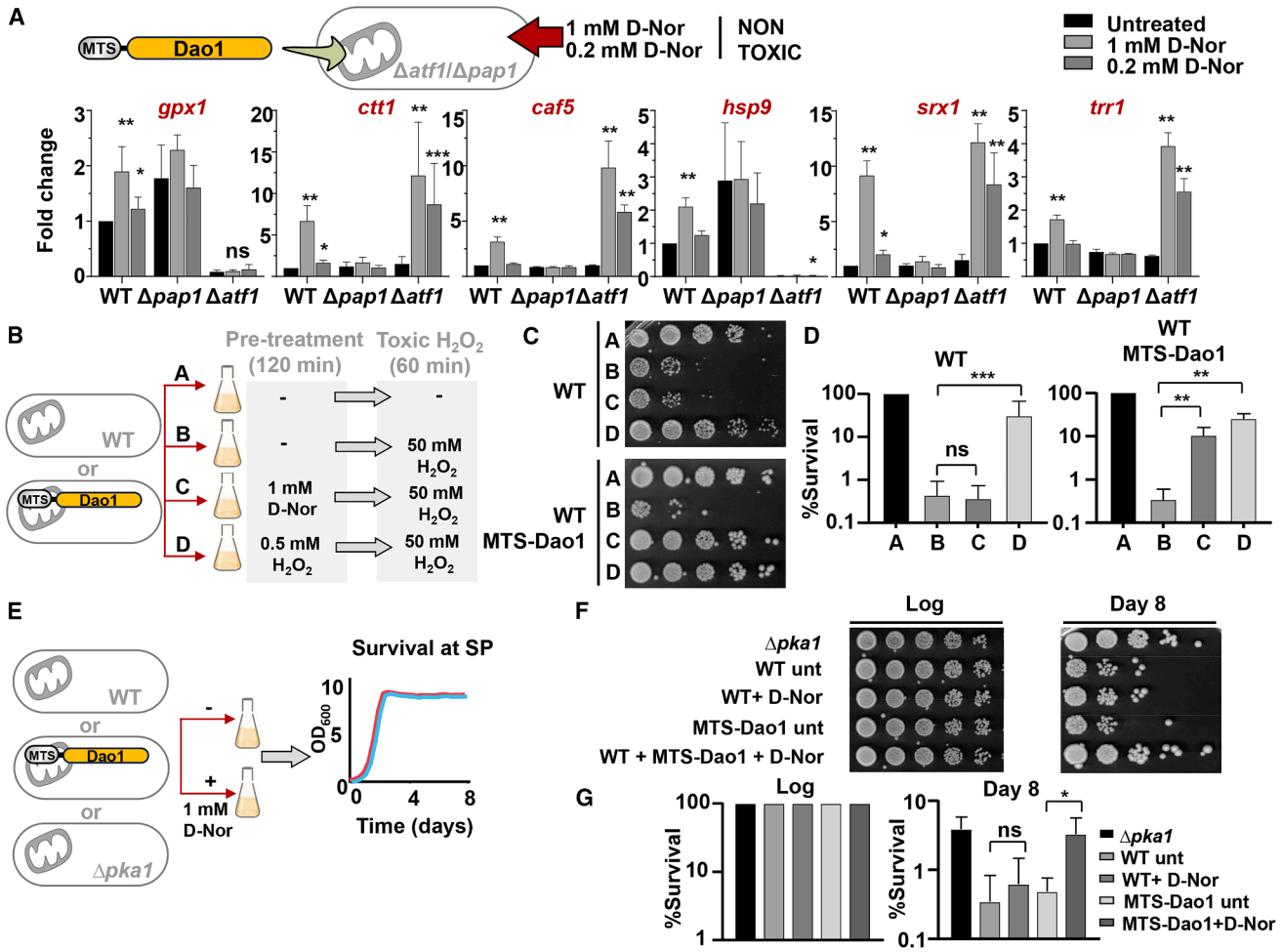

Figure 7. Activation of antioxidant cascades by mitochondria-derived H_2O_2 promoted stress adaptation and extended CLS

(A) Expression of stress genes of strains LC155 (WT), LC124 (Δ*atf1*), and LC162 (Δ*pap1*), all expressing MTS-Dao1, upon treatment with non-toxic concentrations of D-Nor. Experiments were performed and analyzed as described in Figure 6D. For each strain, average data from three biological replicates with error bars are shown. Significant differences between treatments were determined by two-sided *t* test (*$p \leq 0.05$; **$p \leq 0.01$; ***$p \leq 0.001$; ns, not significant).

(B) Scheme depicting the stress-adaptation assay. Cultures of strains expressing (or not) MTS-Dao1 were grown, divided into four flasks, pre-treated or not for 2 h with the indicated concentrations of D-Nor or H_2O_2, followed by stress imposition of 50 mM H_2O_2 for 60 min.

(C) Adaptation assay of strains 972 (WT) and LC154 (WT expressing MTS-Dao1) following the scheme of (B). To monitor survival, cells were spotted in serial dilutions on rich-medium agar plates and grown at 30°C for 2–4 days.

(D) Quantification of spots in (C). The numbers of cells were represented as % survival. Colony counts from the last dilution showing individual colonies were used for quantification. Data were normalized to 100% relative to the untreated condition for each strain. For each strain, data represent the average of three biological replicates with error bars and are presented on a logarithmic scale bar. Significant differences between treatments were determined by two-sided *t* test (**$p \leq 0.01$; ***$p \leq 0.001$; ns, not significant).

(E) Scheme depicting the chronological lifespan (CLS) experiment. Strains expressing (or not) MTS-Dao1 were grown in the presence or absence of 1 mM D-Nor, and the survival was measured comparing samples from logarithmic phase (log) and stationary phase (day 8). Strain FG1 (Δ*pka1*) was used as a long-lived mutant.

(F) CLS assay. Strains 972 (WT) and LC154 (WT expressing MTS-Dao1) were grown following the scheme in (E). The long-lived mutant FG1 (Δ*pka1*) was used as a control. Survival spots were performed as in (C).

(G) Quantification of spots in (F) was performed as described in (D). For each strain, average data from three biological replicates with error bars are shown. Significant differences between treatments were determined by two-sided *t* test (*$p \leq 0.1$; ns, not significant).

See also Figures S8 and S9.

mitochondrial origin could reach the cytosol or nucleus to play a role in signaling. To explore this, we previously used the complex III inhibitor antimycin A, which is known to increase electron leakage and ROS production.[53,54] However, this approach does not generate sufficiently high levels of H_2O_2, and the sensitive biosensor roGFP2-Tpx1.C169S is only minimally oxidized in a WT background.[21] Here, we have shown that MTS-Dao1 can trigger H_2O_2 production and induce either toxicity or beneficial

peroxide fluxes, depending on the concentration of D-amino acids added to the media. Using this H_2O_2-producing system, along with H_2O_2 scavengers and biosensors, we determined that peroxides emanating from the mitochondrial matrix can reach the cytosol and upregulate anti-aging signaling cascades. Two recent studies employed DAOs and H_2O_2 biosensors to investigate peroxide fluxes in mammalian cell lines. Hoehne et al.[55] expressed HyPer7 in various cellular compartments and demonstrated that mitochondria-derived H_2O_2 can diffuse to the cytosol, particularly when major cytosolic peroxiredoxins are inactivated, as we previously reported in fission yeast.[31] However, the physiological implications of these fluxes were not explored in detail. In a complementary study, van Soest et al.[36] fused DAO to either the mitochondrial outer membrane protein Tom20 or to histone H2B and co-expressed these constructs with different HyPer7 isoforms. As in the previous work, close spatial proximity between the H_2O_2 generator and the biosensor was required to detect peroxide fluxes. In this case, nuclear DNA damage was observed upon massive H_2O_2 production by the H2B-DAO chimera, whereas no beneficial effects were reported.

Regarding biosensors, our collection of HyPer7 has allowed us to determine in space and time relative peroxide concentrations based on probe oxidation. Although H_2O_2 was once thought to diffuse freely across membranes, it is now clear that its permeability is not unlimited. H_2O_2-scavenging activities further enhance the differences in concentration between each side of the membrane. By using a combination of HyPer7 derivatives expressed in four different subcellular compartments, we were able to measure relative H_2O_2 concentrations in the nucleus, cytosol, IMS, and matrix and observed how these levels fluctuate following a sudden bolus of H_2O_2, whether initiated from the extracellular space or the mitochondrial matrix. Our data suggest that crossing each intracellular membrane (nuclear, outer, or inner mitochondrial membranes) results in a ~3- to 5-fold reduction in H_2O_2 concentration. It is likely that certain channels or aquaporins contribute to the transport of peroxides across membranes.

Regarding peroxide generation, DAO enzymes are increasingly used as controlled genetic producers of H_2O_2 in living cells, making them a popular tool in redox biology.[36,44,55–58] In using ectopically expressed Dao1 or MTS-Dao1 as chemogenetic tools to induce H_2O_2 bursts, we encountered several issues that required troubleshooting. We carefully monitored the effects of various concentrations of D- or L-amino acids on cell physiology. Two D-amino acids, D-Nor and D-Ala, produced the highest levels of H_2O_2 based on the biosensors. We chose to use D-Nor, expecting to minimize the involvement of amino acid sources in protein synthesis. It was unexpected to find that the control isoform L-Nor exerted toxicity on *S. pombe* cultures, independent of H_2O_2 generation (Figures S5B and S5C). We also observed that high concentrations of D-amino acids, commonly used by researchers, posed a toxic threat to fission yeast cultures when H_2O_2 production was initiated in the mitochondria, causing signs of organelle toxicity (Figures 4 and 5). Notably, when these elevated concentrations of D-Nor were added to rich-yeast-medium cultures, no effect on growth rate was observed (Figure S5E), suggesting that amino acid internalization via permeases, and their accumulation at the plasma membrane from the Golgi apparatus, may vary depending on the medium.

The use of varying concentrations of D-Nor to control H_2O_2 levels helped us visualize the dual effects of ROSs in toxicity and signaling. We determined that 5 and 25 mM D-Nor triggered cytosolic peroxide increases of 0.2–0.3 μM in Dao1-expressing cells, while, in MTS-Dao1-expressing cells, mitochondrial matrix peroxide levels increased by 0.1–0.2 μM (Figure 3F). Toxic effects of H_2O_2 were only observed with the MTS-Dao1 system, suggesting that mitochondria are more sensitive to oxidative stress than the cytosol or that its scavenging systems are less robust. We previously reported that cells lacking Tpx1, which show severe growth defects and equilibrate peroxide levels in both the matrix and cytosol, have steady-state peroxide concentrations around 0.25–0.3 μM.[22] Using mitochondrial and cytosolic biosensors, we proposed that steady-state peroxide levels in the matrix of WT cells are approximately 0.15 μM,[31] as suggested in other model organisms.[32] An increase of 0.1–0.2 μM in MTS-Dao1-expressing cells upon 5–25 mM D-Nor would raise matrix peroxide levels to toxic values, similar to those in strain Δ*tpx1*.

Regarding the use of ectopically expressed peroxide scavengers, we confirmed that the toxicity and signaling effects exerted by MTS-Dao1 upon D-Nor addition were exclusively due to H_2O_2 generation. Accordingly, the expression of MTS-Ctt1 was sufficient to eliminate the mitochondrial toxicity induced by high concentrations of D-Nor in MTS-Dao1-expression cells (Figure 4C). In contrast, MTS-Tpx1 did not confer full protection, likely due to enzyme inactivation caused by the overoxidation of its peroxidatic cysteine.[47,59]

The stress-adaptation- and longevity-promoting effects of low concentrations of D-Nor in MTS-Dao1-expressing strain were abolished by overexpression of both peroxide scavengers in the matrix. As an alternative genetic approach to suppress the beneficial effects of mitochondrial H_2O_2 on fitness and longevity, we deleted the *atf1* or *pap1* genes, both of which encode key components of peroxide-responsive pathways that appear to contribute to lifespan extension. To demonstrate that the beneficial effects of peroxide waves originate from the mitochondria of MTS-Dao1-expressing cells, we conducted several control experiments. Specifically, we showed that, upon addition of 1 mM D-Nor, endogenous *S. pombe* Dao1 did not oxidize the biosensor (Figure S10A), did not induce stress gene activation (Figures S10B and S10C), and cells expressing MTS-Dao1 but lacking endogenous *dao1* displayed cellular adaptation to H_2O_2-induced toxicity upon D-Nor addition (Figures S10D, S10E and S10F).

In conclusion, we demonstrate that these mitochondria-to-cytosol H_2O_2 fluxes can control H_2O_2 cascades at the cytosol. The implications of these findings are important for redox biology and cell physiology. H_2O_2 fluctuations initiated in the mitochondria have been invoked as the cause of diverse (and antagonistic) phenomena such as cancer prevention, metastasis, healthy aging, or cell-differentiation events. We propose that the controlled mitochondrial peroxide fluxes shown here unambiguously separate the toxic and beneficial effects linked to H_2O_2.

Limitations of the study

We used genetic and biochemical approaches to study fluxes of peroxides and their physiological consequences. Findings are based on fission yeast, which may limit direct extrapolation to multicellular eukaryotes or mammalian systems, and the use of other model systems will enhance the translational impact of this work. The use of HyPer7 oxidation values when expressed in different compartments as a readout of H_2O_2 may partially depend on the compartment-specific reduction systems, although we claim that the steady-state levels of peroxides are the main component regulating the starting oxidation values of the biosensors. Although compartment-targeted, diffusion across membranes may blur precise localization of H_2O_2 sources and gradients. Dao1 overexpression and D-amino acid treatment may not fully recapitulate endogenous mitochondrial ROS production dynamics, so other physiological interventions, such as modification of glucose availability, should be used.

RESOURCE AVAILABILITY

Lead contact

Requests for further information and resources should be directed to and will be fulfilled by the lead contact, Elena Hidalgo (elena.hidalgo@upf.edu).

Materials availability

Plasmids and strains generated in this study will be provided upon request from the lead contact.

Data and code availability

- Original data such as images and blots have been deposited in FigShare (https://doi.org/10.6084/m9.figshare.29432840). Additional data reported in this paper will be shared by the lead contact upon request.
- This paper does not report original code.
- Any additional information required to reanalyze the data reported in this paper is available from the lead contact upon request.

ACKNOWLEDGMENTS

We acknowledge Ferran Gómez-Armengol, Itzel Vargas, and Jorge Mallor for the construction of plasmids and strains, and Iria Medraño-Fernández and Ilaria Sorrentino for kindly providing an *Rg*DAO plasmid. We thank NBRP-Yeast for providing strains. This work was supported by grants PID2021-122837-NB-I00 and PID2024-155517-NB-I00 to E.H., funded by MCIN/AEI/10.13039/501100011033 and by "ERDF A way of making Europe," by the European Union. The Oxidative Stress and Cell Cycle Group is also supported by Generalitat de Catalunya (Spain) (2021-SGR-00007) and by the Excellence Unit "María de Maeztu" grant CEX2024-001431-M funded by MCIN/AEI/10.13039/501100011033. E.H. is the recipient of an ICREA Academia Award (Generalitat de Catalunya, Spain). L.d.C. was the recipient of an FPI fellowship from the Ministerio de Economía y Competitividad (Spain), and M.F.C. is the recipient of an FI-Joan Oró fellowship from Generalitat de Catalunya, Spain. Some graphical schemes were created with BioRender.com.

AUTHOR CONTRIBUTIONS

Conceptualization, L.d.C., M.F.C., and E.H.; data curation, L.d.C.; formal analysis, L.d.C., M.F.C., and E.H.; funding acquisition, E.H. and J.A.; investigation, L.d.C., M.F.C., M.V., and S.B.; methodology, L.d.C. and M.F.C.; supervision, E.H. and J.A.; writing – original draft, E.H.; and writing – review & editing, L.d.C., M.F.C., M.V., S.B., J.A., and E.H.

DECLARATION OF INTERESTS

The authors declare no competing interests.

DECLARATION OF GENERATIVE AI AND AI-ASSISTED TECHNOLOGIES IN THE WRITING PROCESS

During the preparation of this work, the authors used ChatGPT in order to improve the readability and language of the manuscript. After using this tool, the authors reviewed and edited the content as needed and take full responsibility for the content of the published article.

STAR★METHODS

Detailed methods are provided in the online version of this paper and include the following:

- KEY RESOURCES TABLE
- EXPERIMENTAL MODEL AND STUDY PARTICIPANT DETAILS
- METHOD DETAILS
  - Generation of plasmids
  - Generation of strains
  - In vivo measurement of basal and induced oxidation of HyPer7 and roGFP-derivatives
  - RNA analysis by reverse transcriptase quantitative PCR (qPCR)
  - Growth curves
  - Microscopy and image analysis
  - Subcellular fractionation and immunoblot analysis
  - TCA extracts and immunoblot analysis
  - Oxygen consumption
  - Chronological lifespan
  - Adaptation to toxic doses of H_2O_2
  - Carbonylation
  - Mitochondrial DNA damage
  - Nuclear DNA damage
- QUANTIFICATION AND STATISTICAL ANALYSIS

SUPPLEMENTAL INFORMATION

Supplemental information can be found online at https://doi.org/10.1016/j.celrep.2026.117277.

Received: September 23, 2025
Revised: February 12, 2026
Accepted: March 26, 2026
Published: April 16, 2026

REFERENCES

1. García-Santamarina, S., Boronat, S., and Hidalgo, E. (2014). Reversible cysteine oxidation in hydrogen peroxide sensing and signal transduction. Biochemistry *53*, 2560–2580. https://doi.org/10.1021/bi401700f.
2. Stöcker, S., Van Laer, K., Mijuskovic, A., and Dick, T.P. (2018). The Conundrum of Hydrogen Peroxide Signaling and the Emerging Role of Peroxiredoxins as Redox Relay Hubs. Antioxid. Redox Signal. *28*, 558–573. https://doi.org/10.1089/ars.2017.7162.
3. Antunes, F., and Brito, P.M. (2017). Quantitative biology of hydrogen peroxide signaling. Redox Biol. *13*, 1–7. https://doi.org/10.1016/j.redox.2017.04.039.
4. Sies, H., and Jones, D.P. (2020). Reactive oxygen species (ROS) as pleiotropic physiological signalling agents. Nat. Rev. Mol. Cell Biol. *21*, 363–383. https://doi.org/10.1038/s41580-020-0230-3.
5. Sies, H., Mailloux, R.J., and Jakob, U. (2024). Fundamentals of redox regulation in biology. Nat. Rev. Mol. Cell Biol. *25*, 701–719. https://doi.org/10.1038/s41580-024-00730-2.
6. Murphy, M.P. (2009). How mitochondria produce reactive oxygen species. Biochem. J. *417*, 1–13. https://doi.org/10.1042/BJ20081386.

7. Holmström, K.M., and Finkel, T. (2014). Cellular mechanisms and physiological consequences of redox-dependent signalling. Nat. Rev. Mol. Cell Biol. *15*, 411–421. https://doi.org/10.1038/nrm3801.

8. López-Otín, C., Blasco, M.A., Partridge, L., Serrano, M., and Kroemer, G. (2023). Hallmarks of aging: An expanding universe. Cell *186*, 243–278. https://doi.org/10.1016/j.cell.2022.11.001.

9. López-Otín, C., and Kroemer, G. (2021). Hallmarks of Health. Cell *184*, 33–63. https://doi.org/10.1016/j.cell.2020.11.034.

10. de Cabo, R., Carmona-Gutierrez, D., Bernier, M., Hall, M.N., and Madeo, F. (2014). The search for antiaging interventions: from elixirs to fasting regimens. Cell *157*, 1515–1526. https://doi.org/10.1016/j.cell.2014.05.031.

11. Chen, K., Shen, W., Gao, Z., and Luo, C. (2021). Stress response capacity analysis during aging and possible new insights into aging studies. Curr. Genet. *67*, 417–420. https://doi.org/10.1007/s00294-021-01159-2.

12. Dawes, I.W., and Perrone, G.G. (2020). Stress and ageing in yeast. FEMS Yeast Res. *20*, foz085. https://doi.org/10.1093/femsyr/foz085.

13. Chance, B., Sies, H., and Boveris, A. (1979). Hydroperoxide metabolism in mammalian organs. Physiol. Rev. *59*, 527–605.

14. St-Pierre, J., Buckingham, J.A., Roebuck, S.J., and Brand, M.D. (2002). Topology of superoxide production from different sites in the mitochondrial electron transport chain. J. Biol. Chem. *277*, 44784–44790. https://doi.org/10.1074/jbc.M207217200.

15. Zuin, A., Carmona, M., Morales-Ivorra, I., Gabrielli, N., Vivancos, A.P., Ayté, J., and Hidalgo, E. (2010). Lifespan extension by calorie restriction relies on the Sty1 MAP kinase stress pathway. EMBO J. *29*, 981–991.

16. Sies, H., Berndt, C., and Jones, D.P. (2017). Oxidative Stress. Annu. Rev. Biochem. *86*, 715–748. https://doi.org/10.1146/annurev-biochem-061516-045037.

17. Winterbourn, C.C., and Hampton, M.B. (2008). Thiol chemistry and specificity in redox signaling. Free Radic. Biol. Med. *45*, 549–561.

18. Leichert, L.I., and Dick, T.P. (2015). Incidence and physiological relevance of protein thiol switches. Biol. Chem. *396*, 389–399. https://doi.org/10.1515/hsz-2014-0314.

19. Zeida, A., Trujillo, M., Ferrer-Sueta, G., Denicola, A., Estrin, D.A., and Radi, R. (2019). Catalysis of Peroxide Reduction by Fast Reacting Protein Thiols. Chem. Rev. *119*, 10829–10855. https://doi.org/10.1021/acs.chemrev.9b00371.

20. Jara, M., Vivancos, A.P., Calvo, I.A., Moldón, A., Sansó, M., and Hidalgo, E. (2007). The peroxiredoxin Tpx1 is essential as a H2O2 scavenger during aerobic growth in fission yeast. Mol. Biol. Cell *18*, 2288–2295.

21. Carmona, M., de Cubas, L., Bautista, E., Moral-Blanch, M., Medraño-Fernández, I., Sitia, R., Boronat, S., Ayté, J., and Hidalgo, E. (2019). Monitoring cytosolic H2O2 fluctuations arising from altered plasma membrane gradients or from mitochondrial activity. Nat. Commun. *10*, 4526. https://doi.org/10.1038/s41467-019-12475-0.

22. Domènech, A., Ayté, J., Antunes, F., and Hidalgo, E. (2018). Using in vivo oxidation status of one- and two-component redox relays to determine H2O2 levels linked to signaling and toxicity. BMC Biol. *16*, 61. https://doi.org/10.1186/s12915-018-0523-6.

23. Paulo, E., García-Santamarina, S., Calvo, I.A., Carmona, M., Boronat, S., Domènech, A., Ayté, J., and Hidalgo, E. (2014). A genetic approach to study H2O2 scavenging in fission yeast–distinct roles of peroxiredoxin and catalase. Mol. Microbiol. *92*, 246–257. https://doi.org/10.1111/mmi.12548.

24. Murphy, M.P., Bayir, H., Belousov, V., Chang, C.J., Davies, K.J.A., Davies, M.J., Dick, T.P., Finkel, T., Forman, H.J., Janssen-Heininger, Y., et al. (2022). Guidelines for measuring reactive oxygen species and oxidative damage in cells and in vivo. Nat. Metab. *4*, 651–662. https://doi.org/10.1038/s42255-022-00591-z.

25. Smolyarova, D.D., Podgorny, O.V., Bilan, D.S., and Belousov, V.V. (2022). A guide to genetically encoded tools for the study of H(2) O(2). FEBS J. *289*, 5382–5395. https://doi.org/10.1111/febs.16088.

26. Hanson, G.T., Aggeler, R., Oglesbee, D., Cannon, M., Capaldi, R.A., Tsien, R.Y., and Remington, S.J. (2004). Investigating mitochondrial redox potential with redox-sensitive green fluorescent protein indicators. J. Biol. Chem. *279*, 13044–13053.

27. Gutscher, M., Sobotta, M.C., Wabnitz, G.H., Ballikaya, S., Meyer, A.J., Samstag, Y., and Dick, T.P. (2009). Proximity-based protein thiol oxidation by H2O2-scavenging peroxidases. J. Biol. Chem. *284*, 31532–31540.

28. Morgan, B., Van Laer, K., Owusu, T.N.E., Ezeriņa, D., Pastor-Flores, D., Amponsah, P.S., Tursch, A., and Dick, T.P. (2016). Real-time monitoring of basal H2O2 levels with peroxiredoxin-based probes. Nat. Chem. Biol. *12*, 437–443. https://doi.org/10.1038/nchembio.2067.

29. Belousov, V.V., Fradkov, A.F., Lukyanov, K.A., Staroverov, D.B., Shakhbazov, K.S., Terskikh, A.V., and Lukyanov, S. (2006). Genetically encoded fluorescent indicator for intracellular hydrogen peroxide. Nat. Methods *3*, 281–286.

30. Pak, V.V., Ezeriņa, D., Lyublinskaya, O.G., Pedre, B., Tyurin-Kuzmin, P.A., Mishina, N.M., Thauvin, M., Young, D., Wahni, K., Martínez Gache, S.A., et al. (2020). Ultrasensitive Genetically Encoded Indicator for Hydrogen Peroxide Identifies Roles for the Oxidant in Cell Migration and Mitochondrial Function. Cell Metab. *31*, 642–653.e6. https://doi.org/10.1016/j.cmet.2020.02.003.

31. de Cubas, L., Pak, V.V., Belousov, V.V., Ayté, J., and Hidalgo, E. (2021). The Mitochondria-to-Cytosol H2O2 Gradient Is Caused by Peroxiredoxin-Dependent Cytosolic Scavenging. Antioxidants *10*, 731. https://doi.org/10.3390/antiox10050731.

32. Cochemé, H.M., Quin, C., McQuaker, S.J., Cabreiro, F., Logan, A., Prime, T.A., Abakumova, I., Patel, J.V., Fearnley, I.M., James, A.M., et al. (2011). Measurement of H2O2 within living Drosophila during aging using a ratiometric mass spectrometry probe targeted to the mitochondrial matrix. Cell Metab. *13*, 340–350. https://doi.org/10.1016/j.cmet.2011.02.003.

33. Sies, H. (2021). Oxidative eustress: On constant alert for redox homeostasis. Redox Biol. *41*, 101867. https://doi.org/10.1016/j.redox.2021.101867.

34. Sies, H. (2020). Findings in redox biology: From H2O2 to oxidative stress. J. Biol. Chem. *295*, 13458–13473. https://doi.org/10.1074/jbc.X120.015651.

35. Murphy, M.P., and O'Neill, L.A.J. (2024). A break in mitochondrial endosymbiosis as a basis for inflammatory diseases. Nature *626*, 271–279. https://doi.org/10.1038/s41586-023-06866-z.

36. van Soest, D.M.K., Polderman, P.E., den Toom, W.T.F., Keijer, J.P., van Roosmalen, M.J., Leyten, T.M.F., Lehmann, J., Zwakenberg, S., De Henau, S., van Boxtel, R., et al. (2024). Mitochondrial H(2)O(2) release does not directly cause damage to chromosomal DNA. Nat. Commun. *15*, 2725. https://doi.org/10.1038/s41467-024-47008-x.

37. Gantner, B.N., Palma, F.R., Kayzuka, C., Lacchini, R., Foltz, D.R., Backman, V., Kelleher, N., Shilatifard, A., and Bonini, M.G. (2024). Histone oxidation as a new mechanism of metabolic control over gene expression. Trends Genet. *40*, 739–746. https://doi.org/10.1016/j.tig.2024.05.012.

38. Palma, F.R., Gantner, B.N., Sakiyama, M.J., Kayzuka, C., Shukla, S., Lacchini, R., Cunniff, B., and Bonini, M.G. (2024). ROS production by mitochondria: function or dysfunction? Oncogene *43*, 295–303. https://doi.org/10.1038/s41388-023-02907-z.

39. Cvetko, F., Caldwell, S.T., Higgins, M., Suzuki, T., Yamamoto, M., Prag, H.A., Hartley, R.C., Dinkova-Kostova, A.T., and Murphy, M.P. (2021). Nrf2 is activated by disruption of mitochondrial thiol homeostasis but not by enhanced mitochondrial superoxide production. J. Biol. Chem. *296*, 100169. https://doi.org/10.1074/jbc.RA120.016551.

40. Sies, H., Belousov, V.V., Chandel, N.S., Davies, M.J., Jones, D.P., Mann, G.E., Murphy, M.P., Yamamoto, M., and Winterbourn, C. (2022). Defining roles of specific reactive oxygen species (ROS) in cell biology and physiology. Nat. Rev. Mol. Cell Biol. *23*, 499–515. https://doi.org/10.1038/s41580-022-00456-z.

41. Krebs, H.A. (1935). Metabolism of amino-acids: Deamination of amino-acids. Biochem. J. *29*, 1620–1644. https://doi.org/10.1042/bj0291620.

42. Pollegioni, L., Diederichs, K., Molla, G., Umhau, S., Welte, W., Ghisla, S., and Pilone, M.S. (2002). Yeast D-amino acid oxidase: structural basis of its catalytic properties. J. Mol. Biol. *324*, 535–546. https://doi.org/10.1016/s0022-2836(02)01062-8.

43. Haskew-Layton, R.E., Payappilly, J.B., Smirnova, N.A., Ma, T.C., Chan, K.K., Murphy, T.H., Guo, H., Langley, B., Sultana, R., Butterfield, D.A., et al. (2010). Controlled enzymatic production of astrocytic hydrogen peroxide protects neurons from oxidative stress via an Nrf2-independent pathway. Proc. Natl. Acad. Sci. USA *107*, 17385–17390. https://doi.org/10.1073/pnas.1003996107.

44. Steinhorn, B., Sorrentino, A., Badole, S., Bogdanova, Y., Belousov, V., and Michel, T. (2018). Chemogenetic generation of hydrogen peroxide in the heart induces severe cardiac dysfunction. Nat. Commun. *9*, 4044. https://doi.org/10.1038/s41467-018-06533-2.

45. Sasabe, J., Miyoshi, Y., Rakoff-Nahoum, S., Zhang, T., Mita, M., Davis, B.M., Hamase, K., and Waldor, M.K. (2016). Interplay between microbial d-amino acids and host d-amino acid oxidase modifies murine mucosal defence and gut microbiota. Nat. Microbiol. *1*, 16125. https://doi.org/10.1038/nmicrobiol.2016.125.

46. Takahashi, S., Okada, H., Abe, K., and Kera, Y. (2012). D-amino acid-induced expression of D-amino acid oxidase in the yeast Schizosaccharomyces pombe. Curr. Microbiol. *65*, 764–769. https://doi.org/10.1007/s00284-012-0227-z.

47. Vivancos, A.P., Castillo, E.A., Biteau, B., Nicot, C., Ayté, J., Toledano, M.B., and Hidalgo, E. (2005). A cysteine-sulfinic acid in peroxiredoxin regulates H2O2-sensing by the antioxidant Pap1 pathway. Proc. Natl. Acad. Sci. USA *102*, 8875–8880.

48. Vega, M., Castillo, D., de Cubas, L., Wang, Y., Huang, Y., Hidalgo, E., and Cabrera, M. (2022). Antagonistic effects of mitochondrial matrix and intermembrane space proteases on yeast aging. BMC Biol. *20*, 160. https://doi.org/10.1186/s12915-022-01352-w.

49. Vivancos, A.P., Jara, M., Zuin, A., Sansó, M., and Hidalgo, E. (2006). Oxidative stress in Schizosaccharomyces pombe: different H2O2 levels, different response pathways. Mol. Genet. Genomics. *276*, 495–502.

50. Veal, E.A., Tomalin, L.E., Morgan, B.A., and Day, A.M. (2014). The fission yeast Schizosaccharomyces pombe as a model to understand how peroxiredoxins influence cell responses to hydrogen peroxide. Biochem. Soc. Trans. *42*, 909–916. https://doi.org/10.1042/BST20140059.

51. Chen, D., Wilkinson, C.R.M., Watt, S., Penkett, C.J., Toone, W.M., Jones, N., and Bähler, J. (2008). Multiple pathways differentially regulate global oxidative stress responses in fission yeast. Mol. Biol. Cell *19*, 308–317.

52. Quinn, J., Findlay, V.J., Dawson, K., Millar, J.B.A., Jones, N., Morgan, B.A., and Toone, W.M. (2002). Distinct Regulatory Proteins Control the Graded Transcriptional Response to Increasing H(2)O(2) Levels in Fission Yeast Schizosaccharomyces pombe. Mol. Biol. Cell *13*, 805–816.

53. Han, D., Williams, E., and Cadenas, E. (2001). Mitochondrial respiratory chain-dependent generation of superoxide anion and its release into the intermembrane space. Biochem. J. *353*, 411–416. https://doi.org/10.1042/0264-6021:3530411.

54. Muller, F.L., Liu, Y., and Van Remmen, H. (2004). Complex III releases superoxide to both sides of the inner mitochondrial membrane. J. Biol. Chem. *279*, 49064–49073. https://doi.org/10.1074/jbc.M407715200.

55. Hoehne, M.N., Jacobs, L.J.H.C., Lapacz, K.J., Calabrese, G., Murschall, L.M., Marker, T., Kaul, H., Trifunovic, A., Morgan, B., Fricker, M., et al. (2022). Spatial and temporal control of mitochondrial H(2) O(2) release in intact human cells. EMBO J. *41*, e109169. https://doi.org/10.15252/embj.2021109169.

56. Halvey, P.J., Hansen, J.M., Johnson, J.M., Go, Y.M., Samali, A., and Jones, D.P. (2007). Selective oxidative stress in cell nuclei by nuclear-targeted D-amino acid oxidase. Antioxid. Redox Signal. *9*, 807–816. https://doi.org/10.1089/ars.2007.1526.

57. Kalinichenko, A.L., Jappy, D., Solius, G.M., Maltsev, D.I., Bogdanova, Y.A., Mukhametshina, L.F., Sokolov, R.A., Moshchenko, A.A., Shaydurov, V.A., Rozov, A.V., et al. (2023). Chemogenetic emulation of intraneuronal oxidative stress affects synaptic plasticity. Redox Biol. *60*, 102604. https://doi.org/10.1016/j.redox.2023.102604.

58. Calabrese, G., Peker, E., Amponsah, P.S., Hoehne, M.N., Riemer, T., Mai, M., Bienert, G.P., Deponte, M., Morgan, B., and Riemer, J. (2019). Hyperoxidation of mitochondrial peroxiredoxin limits H(2) O(2) -induced cell death in yeast. EMBO J. *38*, e101552. https://doi.org/10.15252/embj.2019101552.

59. Bozonet, S.M., Findlay, V.J., Day, A.M., Cameron, J., Veal, E.A., and Morgan, B.A. (2005). Oxidation of a eukaryotic 2-Cys peroxiredoxin is a molecular switch controlling the transcriptional response to increasing levels of hydrogen peroxide. J. Biol. Chem. *280*, 23319–23327.

60. Sansó, M., Gogol, M., Ayté, J., Seidel, C., and Hidalgo, E. (2008). Transcription factors Pcr1 and Atf1 have distinct roles in stress- and Sty1-dependent gene regulation. Eukaryot. Cell *7*, 826–835.

61. de Cubas, L., Boronat, S., Vega, M., Domènech, A., Gómez-Armengol, F., Artemov, A., Lyublinskaya, O., Ayté, J., and Hidalgo, E. (2025). The glutathione system maintains the thiol redox balance in the mitochondria of fission yeast. Free Radic. Biol. Med. *234*, 100–112. https://doi.org/10.1016/j.freeradbiomed.2025.04.012.

62. Vještica, A., Marek, M., Nkosi, P.J., Merlini, L., Liu, G., Bérard, M., Billault-Chaumartin, I., and Martin, S.G. (2020). A toolbox of stable integration vectors in the fission yeast Schizosaccharomyces pombe. J. Cell Sci. *133*, jcs240754. https://doi.org/10.1242/jcs.240754.

63. Alfa, C., Fantes, P., Hyams, J., McLeod, M., and Warbrick, E. (1993). Experiments with Fission Yeast: A Laboratory Course Manual (Cold Spring Harbor Laboratory Press).

64. Brun, C., Dubey, D.D., and Huberman, J.A. (1995). pDblet, a stable autonomously replicating shuttle vector for Schizosaccharomyces pombe. Gene *164*, 173–177.

65. de Cubas, L., Mallor, J., Herrera-Fernández, V., Ayté, J., Vicente, R., and Hidalgo, E. (2023). Expression of the H(2)O(2) Biosensor roGFP-Tpx1.C160S in Fission and Budding Yeasts and Jurkat Cells to Compare Intracellular H(2)O(2) Levels, Transmembrane Gradients, and Response to Metals. Antioxidants *12*, 706. https://doi.org/10.3390/antiox12030706.

66. Bähler, J., Wu, J.Q., Longtine, M.S., Shah, N.G., McKenzie, A., III, Steever, A.B., Wach, A., Philippsen, P., and Pringle, J.R. (1998). Heterologous modules for efficient and versatile PCR-based gene targeting in Schizosaccharomyces pombe. Yeast *14*, 943–951.

67. Castillo, E.A., Vivancos, A.P., Jones, N., Ayte, J., and Hidalgo, E. (2003). Schizosaccharomyces pombe cells lacking the Ran-binding protein Hba1 show a multidrug resistance phenotype due to constitutive nuclear accumulation of Pap1. J. Biol. Chem. *278*, 40565–40572.

68. Sánchez-Mir, L., Fraile, R., Ayté, J., and Hidalgo, E. (2020). Phosphorylation of the Transcription Factor Atf1 at Multiple Sites by the MAP Kinase Sty1 Controls Homologous Recombination and Transcription. J. Mol. Biol. *432*, 5430–5446. https://doi.org/10.1016/j.jmb.2020.08.004.

69. Calvo, I.A., Gabrielli, N., Iglesias-Baena, I., García-Santamarina, S., Hoe, K.L., Kim, D.U., Sansó, M., Zuin, A., Pérez, P., Ayté, J., and Hidalgo, E. (2009). Genome-wide screen of genes required for caffeine tolerance in fission yeast. PLoS One *4*, e6619.

70. Schindelin, J., Arganda-Carreras, I., Frise, E., Kaynig, V., Longair, M., Pietzsch, T., Preibisch, S., Rueden, C., Saalfeld, S., Schmid, B., et al. (2012). Fiji: an open-source platform for biological-image analysis. Nat. Methods *9*, 676–682. https://doi.org/10.1038/nmeth.2019.

71. Chiron, S., Gaisne, M., Guillou, E., Belenguer, P., Clark-Walker, G.D., and Bonnefoy, N. (2007). Studying mitochondria in an attractive model: Schizosaccharomyces pombe. Methods Mol. Biol. *372*, 91–105. https://doi.org/10.1007/978-1-59745-365-3_7.

72. Vivancos, A.P., Castillo, E.A., Jones, N., Ayté, J., and Hidalgo, E. (2004). Activation of the redox sensor Pap1 by hydrogen peroxide requires modulation of the intracellular oxidant concentration. Mol. Microbiol. *52*, 1427–1435.

73. Zuin, A., Gabrielli, N., Calvo, I.A., García-Santamarina, S., Hoe, K.L., Kim, D.U., Park, H.O., Hayles, J., Ayté, J., and Hidalgo, E. (2008). Mitochondrial dysfunction increases oxidative stress and decreases chronological life span in fission yeast. PLoS One *3*, e2842.

74. Boronat, S., Marte, L., Vega, M., García-Santamarina, S., Cabrera, M., Ayté, J., and Hidalgo, E. (2020). The Hsp40 Mas5 Connects Protein Quality Control and the General Stress Response through the Thermo-sensitive Pyp1. iScience *23*, 101725. https://doi.org/10.1016/j.isci.2020.101725.

75. Senoo, T., Yamanaka, M., Nakamura, A., Terashita, T., Kawano, S., and Ikeda, S. (2016). Quantitative PCR for detection of DNA damage in mitochondrial DNA of the fission yeast Schizosaccharomyces pombe. J. Microbiol. Methods *127*, 77–81. https://doi.org/10.1016/j.mimet.2016.05.023.

76. Nakamura, T.M., Du, L.L., Redon, C., and Russell, P. (2004). Histone H2A phosphorylation controls Crb2 recruitment at DNA breaks, maintains checkpoint arrest, and influences DNA repair in fission yeast. Mol. Cell Biol. *24*, 6215–6230. https://doi.org/10.1128/MCB.24.14.6215-6230.2004.

STAR★METHODS

KEY RESOURCES TABLE

REAGENT or RESOURCE	SOURCE	IDENTIFIER
Antibodies		
Anti-GFP monoclonal	Takara	632381; RRID:AB_2313808
Anti-RFP monoclonal	Chromotek	6G6; RRID:AB_2631395
Anti-Tpx1 polyclonal	Laboratory made	Jara et al.[20]
Anti-Tubulin monoclonal	Sigma	T5168; RRID:AB_477579
Anti-H2B-P polyclonal	Abcam	ab17353; RRID:AB_443827
Anti-Sty1 polyclonal	Laboratory made	Jara et al.[20]
Anti-Pap1 polyclonal	Laboratory made	Vivancos et al.[47]
Anti-Atf1 polyclonal	Laboratory made	Sanso et al.[60]
Anti-peroxiredoxin-SO3 polyclonal	AbFrontier	LF-PA0004; RRID:AB_1620996
Anti-Sty1-P (MAPK/p38-P) polyclonal	Cell Signaling Technology	9215; RRID:AB_331762
Bacterial and virus strains		
E. coli DH5a	N/A	N/A
Chemicals, peptides, and recombinant proteins		
Hydrogen peroxide	Sigma	H1009
DTT	Sigma-Aldrich	D0632
D-Norvaline	Thermo Fisher	B23444.14
D-Alanine	Sigma Aldrich	A7377
D-Serine	Thermo Scientific	A1135306
D-Proline	Sigma Aldrich	858919
L-Norvaline	Sigma Aldrich	N7627
L-Alanine	Merck	A7627
L-Serine	Merck	S4500
Zymolyase	Nascalai tesque	7663–91
PMSF	Sigma-Aldrich	P7620
Aprotinin	Sigma-Aldrich	A6279
DNA polymerase	BioTaq, Bioline, Meridian	BIO21040
MitoTracker Red CMXRos	Invitrogen	M7512
Phenol	Sigma Aldrich	33517
TCA	VWR	1,00807,0250
Iodoacetamide	Sigma Aldrich	I1149
FTC	Fluka	46985
Critical commercial assays		
DNAse I	Sigma Aldrich	4716728001
Protease Inhibitor cocktail	Sigma-Aldrich	P8215
RNaseA	Sigma-Aldrich	R5125
Reverse Transcription System	Life technologies	4374966
Light Cycler 480 SYBR Green I Master	Roche	4887352001
Bradford assay	BIO RAD	5000006
Deposited data		
Raw data	FigShare	https://doi.org/10.6084/m9.figshare.29432840
Experimental models: Organisms/strains		
Yeast strains	See Table S1	N/A

(*Continued on next page*)

Continued

REAGENT or RESOURCE	SOURCE	IDENTIFIER
Oligonucleotides		
Primer list	See Table S3	N/A
Recombinant DNA		
p407.C169S	*sty1 prom::roGFP2-Tpx1.C169S*	Carmona et al.[21]
p728	*sty1 prom::HA-HyPer7*	de Cubas et al.[31]
p730	*sty1 prom::MTS^{aco1}-HA-HyPer7*	de Cubas et al.[31]
p836	*sty1 prom::IMS^{cym1}-HA-HyPer7*	This study
p840	*sty1 prom::NLS^{SV40}-HA-HyPer7*	This study
p789.NLS	*sty1 prom::NLS^{SV40}-sfGFP-NLS SV40-sty1*	This study
p838	*sty1 prom::NES^{PKI}-HA-HyPer7*	This study
p699	*sty1 prom::NES^{PKI}-Rho1.C17RGFP*	This study
AY024	*nmt41x′ prom integrative*	Lab stock
p862	*sty1 prom::MBP-HyPer7*	This study
pRgDAO	*RgDAO*	Iria Medraño/Roberto Sitia's labs
p858′	*sty1 prom::HA-RgDAO*	This study
p868′	*sty1 prom::dao1*	This study
p832′	*sty1 prom::MTS^{aco1}-tpx1*	de Cubas et al.[61]
p831′	*sty1 prom::MTS^{aco1}-ctt1*	de Cubas et al.[61]
AY1031	*empty vector ura4 integrative*	Vjestica et al.[62]
p860′	*sty1 prom::MTSaco1-RgDAO*	This study
p853′	*sty1 prom::MTS^{aco1}-dao1*	This study
p903′	*sty1 prom::RgDAO-GFP*	This study
p904′	*sty1 prom::MTS^{aco1}-RgDAO-GFP*	This study
p902′	*sty1 prom::dao1-GFP*	This study
p901′	*sty1 prom::MTS^{aco1}-dao1-GFP*	This study
p906′	*sty1 prom::MTS^{aco1}-ctt1-GFP*	This study
p907′	*nop1 prom::MTS^{aco1}-dao1*	This study
pAY1369	*sty1 prom::MTS^{aco1}-dao1*	This study
Software and algorithms		
Gen5 software	Biotek	N/A
Metamorph 7.8.13	Gataca Systems	N/A
Fiji	NIH; Schindelin 2012	https://imagej.net/software/fiji/
Image Lab	Bio-Rad	N/A
GraphPad Prism (6.0c)	GraphPad Software	https://www.graphpad.com/
BioRender	BioRender	https://www.biorender.com/

EXPERIMENTAL MODEL AND STUDY PARTICIPANT DETAILS

The genotypes of strains used in this study are shown in Table S1. Experiments used haploid isolates of the fission yeast *Schizosaccharomyces pombe* derived from 972 (h^-) or 975 (h^+) strains. *Saccharomyces cerevisiae* strains were derived from BY4741 (*MATa, his3Δ1 leu2Δ0 met15Δ0 ura3Δ0*). No human participants, animals, primary cell cultures, or immortalized cell lines were used in this study, and therefore sex, gender, ancestry, race, and ethnicity are not applicable. No institutional permission or oversight was required. *S. pombe* cells were grown in in rich medium (YE5S) or minimal medium (MM) at 30°C as previously described.[63] For fluorimetry experiments, filtered MM was used to avoid autofluorescence. *S. cerevisiae* strains were grown at 30°C in SD media [yeast nitrogen base (Formedium), 2% glucose], supplemented with 0.1 g/L of methionine, histidine and uracil.

METHOD DETAILS

Generation of plasmids

The plasmids used in this study and their genotypes are provided in Key Resources Table and Table S2. The plasmids described here express fluorescent reporters or H_2O_2 producers under the control of the constitutive *sty1* promoter.[23] Biosensors were expressed

from episomal plasmids, with an average of 7–8 plasmid copies per cell.[64] We used plasmids p407.C169S, p728 and p730 to allow the expression of roGFP2-Tpx1.C169, HyPer7 and MTS-HyPer7, respectively.[21,31] To allow expression of IMS-targeted HyPer7, p836 was created by PCR-amplification from genomic *S. pombe* DNA of the first 86 codons of *cym1* and insertion upstream of *hyper7* in plasmid p728. p840, allowing the expression of NLS^{SV40}-HyPer7, was obtained by restriction enzyme digestion from p789.NLS into p728. p789.NLS codes for a *sty1*-driven NLS^{SV40}-sfGFP-Sty1 in an integrative AY024 backbone. p862 coding for MBP-HyPer7 was constructed by inserting the maltose-binding protein (MBP) into p728. Finally, p838 coding for NES-HyPer7 was constructed by PCR amplifying the *sty1*-promoter and the nuclear export signal of protein kinase inhibitor (NES of PKI) from p699 into p728. p699 codes for a *sty1*-driven NES^{PKI}-Rho1.C17R-GFP in an integrative AY024 backbone. H_2O_2 producers were expressed from integrative plasmids at *leu1* or *ura4* loci. p858′ coding for cytosolic HA-*Rg*DAO was created by Gibson assembly method from a plasmid coding *Rg*DAO (from Iria Medraño and Roberto Sitia lab) and cloned into plasmid AY1031[62] with *sty1* promoter and *nmt1* terminator for integration in *ura4* locus. Plasmid p860′, allowing the expression of MTS-RgDAO, was constructed by restriction enzyme digestion from p858′ and ligation into p831' (*sty1 prom::*MTS^{aco1}*-ctt1*).[61] p853′ and p868′ *ura4* integrative plasmids coding for MTS-Dao1 or Dao1, respectively, under the control of the *sty1* promoter were constructed by restriction enzyme cloning methods. Briefly, Dao1 was PCR-amplified from genomic DNA and cloned into AY1031 with or without MTS^{aco1}. In order to integrate MTS^{aco1}*-dao1* in *leu1* locus, an insert from p853′ was cloned into AY024 backbone yielding pAY1369. For microscopy and mitochondrial fractionation of the different tagged proteins, GFP was PCR-amplified and cloned by Gibson method in the 3′ end of the coding sequences of p858′, p860′, p868′, p853′, p831′ and p832′, yielding plasmids p901′-p904′ and p906′ coding for MTS-Tpx1-GFP, MTS-Dao1-GFP, Dao1-GFP, RgDAO-GFP, MTS-RgDAO-GFP and MTS-Ctt1-GFP, respectively. For expression of MTS^{Aco1}-Dao1 in *S. cerevisiae*, p907 was constructed by PCR amplification of MTS^{aco1}*-dao1* from p853' and cloned into p791.[65]

Generation of strains

The strains used in this study and their genotypes are provided in Table S1. Strains JM13 (*h⁻ dao1::kanMX6*), JM14 (*h⁻ leu1-32 dao1::kanMX6*) and JM16 (*h⁺ dao1::kanMX6 leu1-32 ura4-D18*) were derived from the Δ*dao1* strain in the *S. pombe* haploid deletion collection (Bioneer) by mating with 972 and selecting with or without the appropriate amino acid/s. Similarly, strain FG1 (*h⁻ pka1::kanMX6*) was obtained by mating the Δ*pka1* strain from same collection with strain 972. Strain IV7 (*h⁻ atf1:: natMX6 ura4-D18*) was constructed by homologous recombination using pFA6a-natMX6[66] as template, and inserting the resulting cassette into JA365 (*h⁻ ura4-D18*). For biosensors experiments, strains HM123, JM16 and SG5, were transformed with the indicated plasmids, and selection and growth were performed in MM. Experiments of biosensors combined with cytosolic or mitochondrial expression of RgDAO1 were conducted using in strains JM25 (*h-leu1-32 ura4-D18 sty1'::HA-RgDAO::ura4*) and JM27 (*h⁻ leu1-32 ura4-D18 sty1'::*MTS^{aco1}*-RgDAO::ura4*), generated by integration of plasmids p858′ and p860′ into PN513 (*h⁻ ura4-D18 leu1-32*). Similarly, cytosolic and mitochondrial expression of Dao1 was achieved by integrating plasmids p868′ and p853′ on PN513, yielding LC128 (*h⁻ ura4-D18 leu1-32 sty1'::dao1::ura4*) and LC99 (*h⁻ leu1-32 ura4-D18 sty1'::*MTS^{aco1}*-dao1::ura4*). These strains were subsequently transformed with the corresponding episomal plasmids to express the biosensors. To generate prototrophic strains expressing Dao1 or MTS^{aco1}-Dao1, plasmids p868′ or p853′ were transformed into JA364 (*h⁺ ura4-D18*), yielding LC153 and LC154. Additionally, prototrophic strain LC155 (*h⁻ leu1-32 ura4-D18 MTS*^{aco1}*-dao1::ura4 nmt41x'::leu1*) was generated by transforming LC99 with the empty plasmid AY024. Strains Δ*dao1* and Δ*atf1* expressing MTS^{aco1}-Dao1 were obtained by transformation of JM16 and IV7 with p853′, yielding LC100 (*h⁻ leu1-32 ura4-D18 dao1::kanMX6 MTS*^{aco1}*-dao1::ura4*) and LC124 (*h⁻ atf1::natMX6 ura4-D18 MTS*^{aco1}*-dao1::ura4*), respectively. LC100 was subsequently transformed with AY024 to produce LC157 (*h⁻ dao1::kanMX6 leu1-32 ura4-D18 MTS*^{aco1}*-dao1::ura4 nmt41x'::leu1*). The Δ*pap1* strain LC162 (*h? ura4-D18 leu1-32 pap1::natMX6 MTS*^{aco1}*-dao1::ura4 nmt41x::leu1)* was generated by mating of SG63 (*h⁺ pap1::natMX6 ade6-M216 ura4-D18 leu1-32*) with LC155, followed by selection on MM with antibiotic. For mitochondrial imaging experiments, strain LC164 (*h? ura4-D18 sty1'::MTS*^{aco1}*-dao1::ura4 cpy1-mcherry::kanMX6 sdh2-GFP::natMX6*) was obtained by mating LC99 and MV19 (*h? sdh2-GFP::natMX6 cpy1-mCherry::kanMX6*). For mitochondria fractionation and imaging, strain carrying mitochondrial marker Sdh2-mCherry was transformed with the corresponding plasmids carrying GFP tagged proteins. Strain JA3817 (*h⁻ sdh2-mcherry::natMX6 sty1'::roGFP2-Tpx1.C169S::leu1)* was crossed with strain JA364 yielding MFC24 (*h? ura4-D18 sdh2-mcherry::natMX6*). MFC24 was transformed with plasmids p901′, p902′, p903′, p904′, p906′, and p832′ yielding strains MFC31 (*h? ura4-D18 sdh2-mcherry:: natMX6 sty1'::*MTS^{aco1}*-dao1-GFP::ura4),* MFC32 (*h? ura4-D18 sdh2-mcherry::natMX6 sty1'::dao1-GFP::ura4*), MFC33 (*h? ura4-D18 sdh2-mcherry::natMX6 sty1'::RgDAO-GFP::ura4)*, MFC34 (*h? ura4-D18 sdh2-mcherry::natMX6 sty1'::*MTS^{aco1}*- RgDAO-GFP::ura4*), MFC35 (*h? ura4-D18 sdh2-mcherry::natMX6 sty1'::*MTS^{aco1}*-ctt1-GFP::ura4*), and MFC36 (*h? ura4-D18 sdh2-mcherry::natMX6 sty1'::*MTS^{aco1}*-tpx1::ura4*). Finally, integration of plasmid pAY1369 into PN513 yielded MFC9 (*h⁻ leu1-32 ura4-D18 sty1'::*MTS^{aco1}*-dao1::leu1*). Strain MFC8 (*h⁻ leu1-32 ura4-D18 sty1'::*MTS^{aco1}*-dao1::leu1 sty1'::*MTS^{aco1}*-tpx1::ura4*) was obtained by transformation of MFC9 with p832′, and MFC11 (*h⁺ leu1-32 ura4-D18 sty1'::*MTS^{aco1}*-dao1::leu1 sty1'::*MTS^{aco1}*-ctt1::ura4*) was generated transforming JA312 (*h⁺ leu1-32 ura4-D18*) with pAY1369 and p831'. MFC11 and MFC8 were crossed with a strain containing plasmid p407.C169S, and fluorescent colonies (expressing the biosensor) were isolated in MM.

In vivo measurement of basal and induced oxidation of HyPer7 and roGFP-derivatives

Standard MM-based early stationary phase pre-cultures were diluted in filtered MM to reach an OD_{600} of 1 after 4–5 duplications. We determined the degree of sensor oxidation (OxD) as previously described.[31] D/L-amino acids were freshly prepared in H_2O. In bar graphs, oxidation after 'x' min of treatment (indicated in the Y axis) is represented as OxD or as % OxD; to calculate the OxD, the

average OxD at the indicated time was calculated; to calculate % OxD, data from OxD at the indicated time was rescaled to a percentage, with 100% representing the maximum OxD of the biosensor (OxD = 1) and 0% representing the oxidation at the same time points of untreated cells.

RNA analysis by reverse transcriptase quantitative PCR (qPCR)

Cell cultures at an OD_{600} of 0.5 were harvested after 20 or 30 min, as indicated, treatment with the corresponding D/L-amino acids, and total RNA was extracted by standard phenol method, as described before.[67] Samples were treated with DNAse I followed by reverse transcription using Reverse Transcription System of Applied Biosystems (Thermo Fisher Scientific), as previously described.[68] Quantification of cDNA was performed by real-time quantitative PCR on Light Cycler II using Light Cycler 480 SYBR Green I Master (Roche). For normalization, *act1* gene was used as a control. Primers used are listed in Table S3. Fold induction was calculated comparing the value of each strain and condition to that of the untreated wild-type strain.

Growth curves

Cell cultures at an OD_{600} of 0.5 were diluted in the corresponding media as described above (MM or YE5S for *S. pombe,* SD supplemented with methionine, histidine and uracil for *S. cerevisiae*) to a final OD_{600} of 0.1. Then 100 μL were plated in a 96-well non-coated polystyrene microplate and treated or not with the indicated concentration of D/L-amino acids. The plate was sealed with an adhesive plate seal. Cell growth was monitored for 48 h, with readings every 10 min, with an automatic measurement of optical densities using Power Wave microplate scanning spectrophotometer (Bio-Tek) as previously described.[69] During the whole experiment cells were incubated at 30°C with continuous shaking. The OD_{600} was automatically recorded.

Microscopy and image analysis

Cell cultures were grown until an OD_{600} of 0.5 in MM or YE5S as indicated, then cells were harvested by centrifugation and visualized at room temperature, as previously described.[48] When indicated, small volumes of those cell cultures were incubated with 0.1 μg/mL MitoTracker Red CMXRos (Invitrogen) for 30 min at 30°C in the dark. Cells were centrifuged, and concentrated in its corresponding media for microscopy analysis. Images for biosensors subcellular localization, and mitochondrial morphology using Sdh2-GFP were acquired using z-stacks of 6 images with 0.3 μm spacing. Images were acquired using a Nikon Eclipse 90i microscope equipped with differential interference contrast optics, a PLAN APO VC 100 × 1.4 oil immersion objective, an ORCA-II-ERG camera (Hamamatsu), excitation and emission filter GFP-4050B, mCherry-C (Semrock), and image acquisition software Metamorph 7.8.13 (Gataca Systems). For experiments to analyze the subcellular localization and co-localization of GFP-tagged proteins with the mitochondrial marker Sdh2-mCherry brightfield and fluorescence images were acquired with a Nikon Eclipse Ti2-E inverted microscope equipped with a 100X/1.45 NA objective (Nikon). GFP and mCherry signals were detected using SpectraX Lumencor LED illumination system, with excitation filters of 475/35 nm (Semrock) for GFP and 575/35 nm (Chroma) for mCherry, and FF01-524/628-25 dual band-pass emission filter (Semrock). For analysis, mitochondrial images of Sdh2-GFP were then deconvolved, and represented as maximum-intensity projections. Processing of all images was performed using Fiji (ImageJ, National Institutes of Health).[70]

Subcellular fractionation and immunoblot analysis

Whole-cell extracts (WCE), cytosolic (CYT), and mitochondrial (MIT) fractions were obtained from exponentially growing *S. pombe* cells using a differential centrifugation protocol as previously described[71] with some modifications. Cells were grown in 1 L of YE5S medium to an OD_{600} of ∼0.7, harvested by centrifugation at 2,000 × g for 10 min at room temperature, and washed once with distilled water. Cell pellets were resuspended in 50 mL 10 mM EDTA and centrifuged at 2,000 × g for 10 min at room temperature prior to enzymatic digestion. Protoplasts were generated by resuspending cells at 3 mL per gram of wet weight in digestion buffer (1.2 M sorbitol, 10 mM sodium citrate, 0.4 mM EDTA) supplemented with 2 mg/mL zymolyase and incubated for 1 h at 37°C with gentle shaking. Digestion was stopped by cooling on ice, and all subsequent steps were performed at 4°C using ice-cold buffers. Protoplasts were pelleted at 2,000 × g for 5 min and lysed in lysis buffer (0.6 M sorbitol, 10 mM imidazole, 4 mM EDTA) using a glass homogenizer (10 strokes). Unbroken cells and debris were removed by centrifugation at 2,500 × g for 5 min. One mL of supernatant was kept at this step as a whole-cell extract (WCE) fraction. The rest of the supernatant was centrifuged at 12,000 × g for 5 min to separate the organelle fractions from the cytosolic fraction (CYT fraction). The mitochondrial pellet was washed once by resuspension in lysis buffer followed by centrifugation at 800 × g and 12,000 × g twice to concentrate mitochondrial protein content. Finally, the pellet was resuspended in 100 μL of lysis buffer (MIT fraction). Protein concentrations were determined by Bradford assay. The indicated μg of total protein from WCE, CYT, and MIT fractions were resolved by SDS–PAGE and analyzed by immunoblotting using antibodies against GFP, RFP, Tpx1 and tubulin, the latter serving as a cytosolic marker and loading control.

TCA extracts and immunoblot analysis

Modified trichloroacetic acid (TCA) protein extracts were prepared as previously described.[47] Briefly, 10% TCA was added to cell cultures to allow protein precipitation, after vortex TCA was washed with acetone. Pellets were resuspended in Tris-buffer (1% SDS, 100 mM Tris·HCl pH 8, 1 mM EDTA) with or without 75 mM iodoacetamide. Samples with alkylating agent were incubated

for 15 min at 25°C. Proteins were separated by SDS-PAGE under reducing or non-reducing conditions depending if samples were not alkylated or alkylated respectively. Proteins were detected by immunoblotting with a polyclonal anti-Pap1,[72] anti-Tpx1,[20] anti-Atf1,[60] anti-peroxiredoxin-SO_3 antibody (AbFrontier, Seoul, South Korea) and anti-Sty1-P (MAPK/p38-P; Cell Signaling Technology, 9215). StartBright Blue 700 Fluorescence anti-Rabbit secondary antibody (Bio-Rad) was used for quantification. Finally, visualization was performed using ChemiDoc MP Imaging System (Bio-Rad, 12003154).

Oxygen consumption

Oxygen consumption was performed as described previously.[73] Briefly, cells were treated with the indicated concentrations of D/L-amino acids during the indicated times. Then cells were harvested, and 2×10^7 cells were resuspended in 1 mL of MM to a final OD_{600} of 1. Measurements were made using a Hansatech Oxygraph (Hansatech), with readings being recorded during 10 min. Each one of the measurements was performed from biological triplicates.

Chronological lifespan

To test lifespan, cells were grown in MM at 30°C. Stationary phase precultures were diluted and grown overnight in MM with or without 0.5 mM D-Nor. Control strain FG1 (Δ*pka1)* was directly inoculated in MM. When OD_{600} of 0.5 was reached, cultures were treated or not with 1 mM of D-Nor. During the course of the experiment, cell samples were harvested at the indicated days. The same concentration of cells (OD_{600} 2.5) was spotted in 1/10 serial dilutions in YE plates and incubated at 30°C for 2–4 days.

Adaptation to toxic doses of H_2O_2

Cells grown in MM until an OD_{600} of 0.5 were treated for 120 min with 1 mM D-Nor, 0.5 mM H_2O_2 or left untreated. Then 50 mM of H_2O_2 was applied for 60 min. Cells were harvested and plated as described above in YE plates to monitor survival.

Carbonylation

Total protein carbonylation was determined by fluorescein thiosemicarbazide derivatization of protein extracts, as previously described[74] with minor modifications. Briefly, 50 mL of logarithmically growing cells in MM were treated with 25 mM D-Nor for 16 and 24 h or with 2.5 mM H_2O_2 for 4 h or left untreated. Protein extracts were prepared and derivatized as previously described.[74] To visualize protein carbonylation, 20 μg of the derivatized protein extracts were loaded in 12% SDS-PAGE. Gels were scanned using an Amersham Typhoon scanner (Cytiva) with a 532 nm filter at 850 V. Total protein was determined by silver staining and using the image acquisition ChemiDoc MP Imaging System (Bio-Rad, 12003154). Quantification was performed using the Image Lab (Bio-Rad) software.

Mitochondrial DNA damage

Mitochondrial DNA damage was quantified as previously described without isolation of mitochondria and mitochondrial DNA.[75] Total DNA from Dao1-or MTS-Dao1-expressing cells, treated or not with D-Nor, was obtained. Briefly, 20 mL of cells grown in MM were harvested at OD_{600} of 0.5, washed and resuspended in ice-cold DNA extraction buffer [2% Triton X-100, 1% SDS, 100 mM NaCl, 10 mM Tris-HCl (pH 8.0), 1mM EDTA]. After adding same volumes of phenol and chloroform cells were lysed with glass beads in a Minibeadbeater-16 (Biospec products, Bartsville) with 3 pulses of 45 s each. The aqueous layer was cleaned with chloroform. DNA in the final aqueous phase was precipitated at −80°C by adding 1/10 volume 3 M sodium acetate (pH 5.2) and 2.5 volume 100% ethanol. DNA pellet was washed with 70% ethanol and resuspended in TE buffer. RNA was degraded by treating at 37°C for 30 min with a final concentration of 0.25 μg/μL of RNaseA. Before PCR, DNA was quantified by agarose gel electrophoresis. 1 ng of template was used for mitochondrial DNA amplification with primers spanning 2.1 kb (to highlight DNA damage) or 0.15 kb (as an indication of relative mitochondrial DNA copy number). PCR reactions were performed in 25 μL with 2.5 mM magnesium chloride, 0.8 μM of each oligo, 0.1 mM dNTPs and 0.625 U of DNA polymersase (BioTaq, Bioline, Meridian, BIO21040). As a control of oxidative toxicity, samples from cultures exposed for 6 h to 5 mM of H_2O_2 were used.

Nuclear DNA damage

As an indication of nuclear DNA damage we measured the phosphorylation of histone H2A (H2A-P).[76] Briefly, 40 mL of cells untreated or treated with H_2O_2 or D-Nor were collected and resuspended in 0.25 mL of lysis buffer [1 x PBS, 0.2 M NaCl, 0.5 mM EGTA, 0.5 mM EDTA, 0.1% Triton X-100, and PMSF, aprotinin, PIC (protease inhibitor cocktail) as protease inhibitors]. Cells were lysed with glass beads using a Biospec minibeadbeater and 3 ×45 s cycles. Protein extracts were clarified by a 10 min centrifugation and quantified by Bradford assay. 20 μg of total protein were loaded in 15% SDS-PAGE and transferred to nitrocellulose membranes. Membranes were cut and the lower part was blocked with 3% BSA, to detect H2A-P using an anti gammaH2A antibody (ab17353, Abcam) and the upper part was blocked with 3% non-fat dry milk to detect Sty1 with a home-made Sty1 antibody[20] to be used as loading control.

QUANTIFICATION AND STATISTICAL ANALYSIS

For *in vivo* fluorescence probe oxidation quantification, OxD, independent cultures of the strains of interest were grown for each replicate. In all figure panels, values of mean of $n = 3$ are shown with error bars represented as standard deviation. Statistics were performed with a Student *t* test. For western blots and microscopy images, a representative experiment is shown from at least three biological replicates.